Quantum Dot-Polymer Interactions in Contact Electrification of Common Polymers

A THESIS SUBMITTED TO
THE GRADUATE SCHOOL OF ENGINEERING AND SCIENCE
OF BILKENT UNIVERSITY
IN PARTIAL FULFILLMENT OF THE REQUIREMENTS FOR
THE DEGREE OF
MASTER OF SCIENCE
IN
MATERIALS SCIENCE AND NANOTECHNOLOGY

By

Görkem Eylül KAYA

August 2023

QUANTUM DOT-POLYMER INTERACTIONS IN CONTACT ELECTRIFICATION OF COMMON POLYMERS

By Görkem Eylül Kaya

August 2023

We certify that we have read this thesis and that in our opinion it is fully adequate, in scope and in quality, as a thesis for the degree of Master of Science.

_____

Bilge Baytekin (Advisor)

_____

Demet Asil Alptekin

_____

Aykut Erbaş

Approved for the Graduate School of Engineering and Science:

_____

Orhan Arıkan
Director of the Graduate School

ABSTRACT

Quantum Dot-Polymer Interactions in Contact Electrification of Common Polymers

Görkem Eylül Kaya

M.S. in Materials Science and Nanotechnology

Advisor: Bilge BAYTEKIN

August 2023

Contact electrification or static charging occurs when we rub or contact insulator surfaces. This contact leads to the development of electrical charges, and accumulation of these charges may lead to uncontrolled electrostatic discharging (ESD), causing accidents, e.g., powder explosions, and economic losses in the industry. Conversely, contact charges can contribute to many application fields, such as recently developed triboelectric nanogenerators for harvesting mechanical energy. Therefore, it is crucial to control contact charges by knowing the mechanisms of contact electrification in dept. However, despite centuries of research, there are still many debates and unknowns in contact charging of polymers since it has many complex events such as electron, ion and material transfer between the surfaces. In this thesis, we studied the contact electrification of common polymers doped with quantum dots (QDs). Surface engineering of polymers at the nanoscale can open doors for new applications and give insights into contact electrification. In the first part of the thesis, we investigated the mitigation mechanisms of contact charges by doping CdS_xSe_{1-x} and CdS_xSe_{1-x}/ZnSe QDs into PDMS polymer. We tested the interaction of QDs with the polymer based on the different locations of charge carriers (electrons and holes) via a band-gap engineering approach. In the following sections of the thesis, we studied the contact charge generation in the QD-polymer composites, initially by testing the effect of ligand exchange treatment on QDs by pyridine treatment of QDs capped with oleic acid. Then,

the effect of different polymer matrices was tested by doping QDs into polyethylene, polystyrene, and polymethyl methacrylate. In the last section of the thesis, nitrogen-doped carbon dots - a more biocompatible and environmentally friendly additive compared to inorganic QDs - were doped into polyvinyl alcohol to study contact charge generation. QDs and QD-doped polymers were characterized by UV-VIS spectroscopy, photoluminescence, time-resolved fluorescence, atomic force microscopy, transmission electron microscopy, and X-ray diffractometry. It was demonstrated that QDs can be used to stabilize or destabilize the contact charges on the surfaces, and this effect can be further manipulated by UV light illumination. This first-time display of the light-tunability of static charges in common polymers might help prevent excessive accumulation of charges on them or enhance the static charge stability on demand. Finally, we believe our results can be beneficial to enlighten the physical interactions of QDs with common polymers at the nanoscale and may be used to design straightforwardly-accessible materials having advanced electronic properties.

ÖZET

Dokunma ile Elektriklenmede Kuantum Noktaları-Polimer Etkileşimleri

Görkem Eylül Kaya
Malzeme Bilimi ve Nanoteknoloji, Yüksek Lisans
Tez Danışmanı: Bilge BAYTEKIN
Ağustos 2023

Dokunma ile elektriklenme, yalıtkan bir malzeme yüzeyinin başka bir yüzeye dokundurulması veya sürtünmesi ile meydana gelir. Bu temas, elektrik yüklerinin oluşmasına neden olur ve bu yüklerin birikmesi kontrolsüz elektrik deşarjına yol açarak örneğin, deşarj kaynaklı toz patlamaları gibi kazalara neden olur. Bu ve benzeri durumlar endüstride ciddi ekonomik kayıplara yol açar. Öte yandan, oluşan bu elektrik yükleri, son zamanlarda gelişen triboelektrik nanojeneratörler gibi mekanik enerjinin elde edilmesinde kullanılan bir çok uygulama alanına katkıda bulunabilir. Bu nedenlerle, dokunma ile elektriklenme sonrasında oluşan yüklerin kontrolünü sağlamak ve elektriklenme mekanizmasını detaylı olarak anlamak önem taşımaktadır. Ancak dokunma ile elektriklenme, yüzyıllarca süren araştırmalara rağmen hala tam olarak anlaşılamamıştır çünkü elektron, iyon ve malzeme transferi gibi karmaşık olaylar içerir. Bu tezde, kuantum noktaları (KN'ler) yaygın olarak kullanılan polimerlere eklenmiş, polimerlerin dokunma ile elektriklenmesi incelenmiştir. Nanometre ölçeğindeki yüzey mühendisliği, bu KN-polimer kompozitleri için yeni uygulama alanları yaratabilir ve dokunma ile elektriklenmenin mekanizmasının aydınlatılmasına yardımcı olabilir. Bu tezin ilk bölümünde, CdS_xSe_{1-x} ve CdS_xSe_{1-x}/ZnSe KN'lerini PDMS polimerine ekleyerek oluşan kompozit elektriklendirildiğinde oluşan yüklerin sönümlenme mekanizmalarını araştırılmmıştır. KN'lerin polimerle etkileşimlerini, elektron-boşluk yük taşıyıcılarının farklı konumlarına göre, bant genişliği mühendisliği yaklaşımıyla

test edilmiştir. Tezin diğer bölümlerinde, KN-polimer kompozitlerinde yük oluşumu incelenmiştir. Öncelikle oleik asit ile kaplanmış KN'leri piridin ile işleme tabi tuttuk ve böylece KN'lerdeki ligand değişim işleminin yüklenmeye etkisi test edilmiştir. Daha sonra, farklı polimer matrislerinin yük stabilitesine etkisi, polietilen, polistiren ve polimetilmetakrilat polimerlerine KN katkılanarak araştırılmıştır. Tezin son bölümünde ise, inorganik KNlere kıyasla daha biyo-uyumlu ve çevre dostu bir katkı madde olan azot eklenmiş karbon noktaları polivinil alkol polimerine eklenerek yüklenme deneyleri yapılmıştır. KNler ve KNli polimerler UV-VIS spektroskopisi, fotolüminesans, ışıma ömrü, atomik kuvvet mikroskopisi, transmisyon elektron mikroskopisi ve X-ışını kırınımı yöntemleriyle karakterize edilmiştir. Sonuç olarak KNlerin, polimer yüzeylerindeki yükleri stabilleştirme veya kararsızlaştırma amacıyla kullanılabileceği ve bu etkilerin UV ışığı ile aydınlatma sayesinde de manipüle edilebileceği görülmüştür. Bu tez çalışması ile, yaygın olarak kullanılan plastiklerde statik yüklerin ışıkla manipüle edilebileceği literatürde ilk defa göstermiştir. Bulduğumuz sonuçlar, polimer yüzeylerde aşırı yük birikimini önlemeye veya isteğe bağlı olarak statik yük stabilitesini artırmaya yönelik uygulamalara fayda sağlayabilir. Son olarak, sonuçlarımızın, kuantum noktalarının yaygın polimerlerle nanometre ölçeğindeki fiziksel etkileşimlerini aydınlatmada faydalı olduğuna ve gelişmiş elektronik özelliklere sahip yeni kolay erişilebilir malzemeler tasarlamak için kullanılabileceğine inanıyoruz.

Acknowledgments

I would like to sincerely thank everyone who has been involved in the completion of my master's degree.

First and foremost, I am deeply grateful for having a chance to work with my advisor, Assoc. Prof. Bilge Baytekin's research group. I sincerely thank her for all her guidance and support throughout my master's studies.

I am very grateful to Assoc. Prof. H. Tarık Baytekin for his guidance and support in my experiments and for welcoming me into his laboratory. I would like to thank Asst. Prof. Demet Asil Alptekin for her support in the preparation of quantum dots and her guidance in my thesis work. I would like to thank Asst. Prof. Erol Yıldırım for his valuable theoretical calculations and support.

I sincerely thank the jury members of my thesis committee, Asst. Prof. Aykut Erbaş and Asst. Prof. Demet Asil Alptekin, for their constructive feedback and for sparing time to evaluate my thesis.

I would like to thank all current and former members of the Baytekin research group, especially Sunay Dilara Ekim and Pedram Tootoonchian, for always being helpful throughout my research and for their wonderful friendship. I thank Firdevs Aydin for the preparation of quantum dots and her support.

Finally, I would like to thank Alper Dağgez, my family, and all of my lojman friends for being my constant source of motivation. Their support and belief in me have been incredibly valuable.

The Scientific and Technological Research Council of Turkey (TUBITAK) for financial support under project no: 120M694

For my mother,

Table of Contents

Figure List

"Out of clutter, find simplicity. From discord, find harmony. In the middle of difficulty lies opportunity."

Albert Einstein

Chapter 1

1. INTRODUCTION

1.1.What is contact electrification?

Contact electrification (static charging) occurs when two identical [1], [2], or different surfaces [3] are contacted and separated. It is a universal phenomenon as it appertains to nearly all types of materials, such as metals, inorganic materials, semiconductors, and polymers. As a result of this contact, electrical charges are developed on the surfaces. Accumulation of these charges can be undesirable, especially in our daily lives, such as dust sticking to electronic screens or small shocks when touching other people or metals. [4]–[6] More importantly, this accumulation can cause significant electrostatic discharge problems, such as the breakdown of electronic circuitry, or electrostatic explosions, all of which result in substantial financial losses for industry, [7].

On the contrary, contact electrification can also be beneficial in some applications such as particle separation [8], laser printing [9], and the recently developed triboelectric nanogenerators to harvest mechanical energy [10].

In order to extend the range of applications, a detailed understanding and research into the molecular mechanism of contact electrification is necessary. Despite centuries of research on the molecular mechanism of contact electrification, There are still many unknowns in contact charging of polymers since it involves complex events such as electron and ion transfer [11]–[13] and material transfer [14], [15] between the surfaces. These events are also affected by many variables, such as the surface distribution of charges and environmental conditions. [16]

1.2. Possible mechanisms of contact electrification

Most studies in contact electrification focus on the electron and ion transfer mechanisms, and these mechanisms have been prominent in the past decade. The electron transfer mechanism describes that contact leads to the redistribution of charges on the contacting surfaces based on the different work functions of the materials. According to this mechanism, the electrons are transferred from the material with a low work function to the material with a higher work function to equalize the Fermi levels of materials to establish a thermodynamic equilibrium. [16], [17]. This mechanism is predominantly accepted for the electrification of two metal surfaces, or a metal and an insulator surface.

The ion transfer mechanism interprets the exchange of protons or ions between the surfaces after contact, leading to charge separation. Especially in insulating materials with different acidity/basicity properties and mobile ions, ion transfer might be prevailing. [18] The possible electron and ion transfer mechanisms in contact electrification are schematically shown in Figure 1.1.

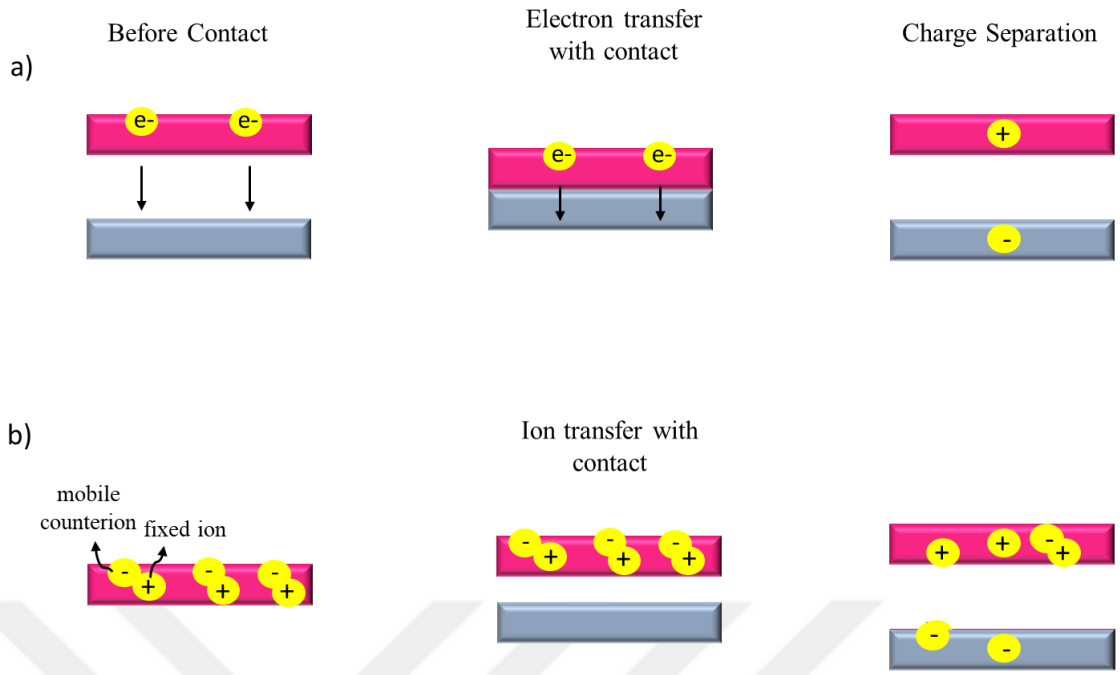

Figure 1.1. The schematic illustration of the electron and ion transfer mechanisms of contact-charging of two surfaces. a) Electron and b) Ion transfer mechanisms.

The electron and ion transfer mechanisms alone fail to explain the exact mechanism of contact electrification, especially for the insulator-insulator contacts. In insulators, electron transfer is hindered due to the large energy barrier between their highest occupied molecular orbitals (HOMO) and lowest unoccupied molecular orbitals (LUMO), so the electron transfer mechanism is not enough to answer what the source of electrons in insulators is. Moreover, not all insulators have readily available mobile ions on their surfaces, and it has been observed that insulators can still become contact charged in high vacuum conditions or in the absence of air/water without needing external ions. [19]–[21] Therefore, ion transfer mechanism is also insufficient to enlighten the overall mechanism of contact electrification.

Recent reports revealed that material transfer plays a significant role in contact charging. Bond cleavages on the contact-charged surfaces of polymers generate mechanoions and mechanoradicals on the surface of materials and mediates the

materials transfer. [7], [22], [23] The mechanism of contact electrification cannot be explained with a single mechanism, the studies so far point out to a combination of different mechanisms. This combined mechanism suggests that the charge is generated on the surface by bond scission (cleavage) upon mechanical input. The cleavage forms the broken polymer chains, called as the 'mechanospecies'. The mechanospecies include mechanoanions and mechanocations (the – and + charges observed as contact charges) and mechanoradicals. These mechanospecies may interact with the surrounding chemical species. Their interactions with the surrounding chemical environment can explain the related electron, ion, and material transfer between the surfaces. In the context of this hypothesis, Sakaguchi et al. provided an initial study showing that electrons can be transferred among mechanoanions, mechanocations, and mechanoradicals that are generated on the surfaces of polymer. [12] Later the existence of a mosaic surface was demonstrated by Baytekin et al. [4] Kelvin probe force microscopy was utilized to visualize contact charges on polymer surfaces, revealing a mosaic structure composed of positive and negative charge nanodomains. A following study by the same group revealed that the mechanospecies indeed intearact and stabilize each other, and chemical removal of mechanoradicals for example can destabilize mechanoions, and render material permanently antistatic [7]. Another study showed that the natural radical scavengers can interact with mechanospecies on the surfaces of the contact-charged synthetic polymers. [24] It was also shown that wood owes its super antistatic nature to the mechanospecies/lignin interaction [25] The sensitivity of the mechanospecies to the surrounding environment's polarity was displayed and this sensitivity was used to manipulate these species by light, too. [26] The chemical interactions among the mechanospecies was described by calculations. [27] Recently, a correlation is established between the cohesive energy densities of surfaces and their

triboelectrification behavior. [28] These studies propose that bond scission of the polymers forms charged species (mechanoions) as the contact charges on the surface of polymers, and that they can interact with each other and surrounding chemical species.

1.3. Triboelectric Series

Triboelectric series is a well-known way to treat contact-charging of the materials. In triboelectric series, ranking is made from the material having a higher tendency to become positively charged (lose electron) to the material with a tendency to become negatively charged (gain electron) upon contacting each other. The first triboelectric series was published in 1757 by J.Carl Wilcke, [29] Wilcke listed materials according to their ability to gain or lose electrons in the order of polarity. Many triboelectric series have been published over the past 150 years by covering a wider range of materials. [30]–[32] While these published series generally agree with one another, some inconsistencies exist caused by the different compositions of prepared materials, preparation environment, and processing history of the material. In addition, materials charge bipolarly in nano [4], micro, and macrodomains [33], [34], meaning that not all charges on the surface are completely positive or negative, therefore making the utility of triboelectric series limited. For a rough selection of materials, for example, a material couple for building a triboelectric energy harvester can be selected form the series' positive and negative ends. Nevertheless, this series is far from explaining any mechanisms at the molecular level, therefore we refrain from discussions involving the triboelectric series in this work.

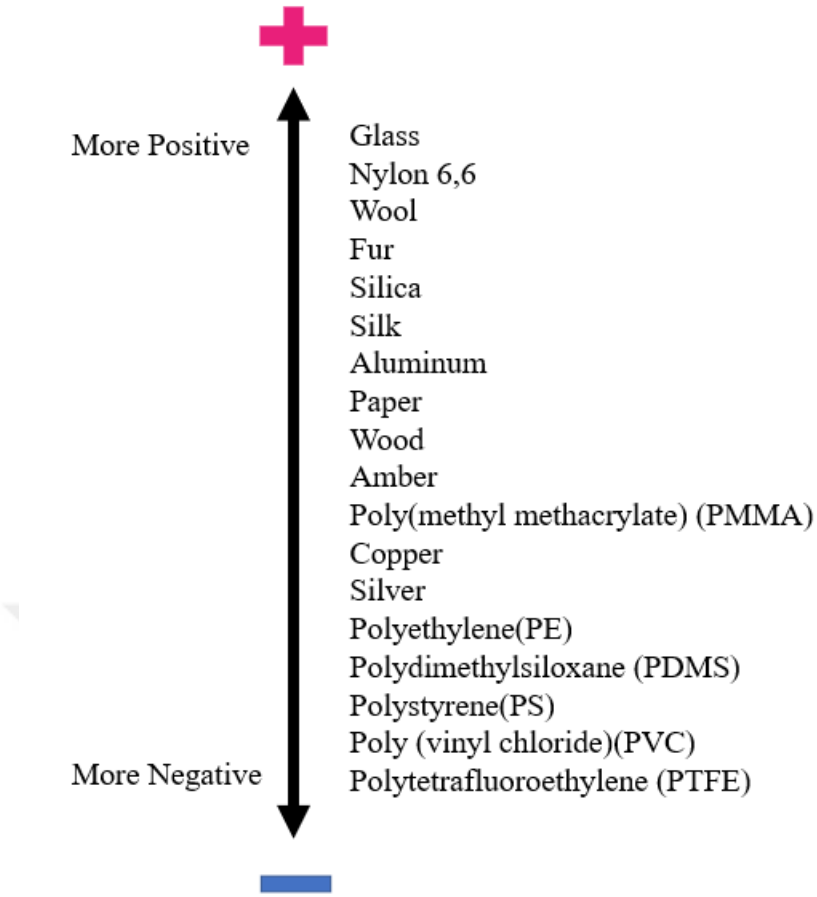

Figure 1.2. A triboelectric series of materials

1.4. Controlling contact electrification

Contact electrification of polymer materials is overly sensitive to surface states and environmental factors. Environmental factors, such as humidity and temperature, have been widely studied as the most effective factors in tribocharging. [35]–[38] The contact method (e.g., rubbing or contacting), the amount of pressure applied, and the property of materials such as size, roughness and purity are also important factors in affecting the contact electrification. [39], [40] Utilizing the triboelectric chart is a rough approach to selecting a material with desired charging properties. The desired charging properties can also be achieved by incorporation of various additives in the materials.

The choice of additives is diverse. There are additives to enhance or decrease polymer contact electrification.

1.4.1. Charge Mitigation

As described before, the accumulation of charges on the surfaces can be detrimental to many industries. Therefore, developing antistatic materials is crucial for many applications. Doping the materials with antistatic agents can effectively eliminate charge accumulation. Antistatic agents such as metals [41], carbon nanotubes [42], conductive ionic liquids [43], and conductive polymers [44] can eliminate the accumulation of surface charges. These additives have to be doped in large amounts (typically 10% - 40%) in order to ensure the 'antistatic limit' reached by the conductivity increase upon doping. Therefore, the doping usually alters the other, desired properties of materials; the mechanical and electrical properties are affected. As explained above, recent studies showed an approach that considers how the charges form and are stabilized/destabilized on the surfaces can be beneficial over the traditional doping techniques. For example, doping polymers with radical scavengers make them antistatic without increasing the conductivity– keeping the polymer electrically insulating. The doping amounts are usually low (up to a few percent only), which does not change the mechanical properties of the material. The mechanism of the antistatic action with radical scavengers and similar chemicals are explained as follows [7]: When two materials are contacted, mechanoions and mechanoradicals are generated due to the mechanochemical bond cleavage [4], [7]. Mechanoradicals can stabilize the mechanoions (charges) and lead to the accumulation of charges on the surface [7]. If some radical scavengers were previously added to the pristine material, these scavengers react with the mechanoradicals forming through mechanochemical

breakages. The removal of the mechanoradicals destabilizes the mechanoions, resulting in faster charge dissipation. In summary, this new method focuses on the charge destabilization instead of increasing the conductivity of the surfaces. The doping of the materials with radical scavengers such as vitamin E [7], lignin [25], organic dyes [26], and organic charge transfer complexes [45] have achieved remarkable results in developing new antistatic materials.

1.4.2. Charge Generation

As described above, charge accumulation can be beneficial to several industrial applications. Enhancing surface charges is crucial for efficient triboelectric nanogenerator (TENG) applications. A TENG is an energy generator that transforms mechanical energy into electrical energy using contact electrification at the nanoscale. [10] TENG technology has some advantages compared to other technologies, such as high efficiency, low cost, and a simple fabrication process. Various attempts have been made to improve TENG performance, including incorporation of additives into the polymers used in these devices. Additives such as Au nanoparticles [46], TiO_2 [47], and bio-degradable additives such as starch [48] and keratin [49] have been shown to improve the voltage output. Graphene quantum dots were also used successfully to enhance the electrical voltage output of nanogenerators. [50]

1.5.Semiconductor Quantum Dots

Quantum dots (QDs) are semiconductor nanocrystals comprising an inorganic core and an organic outer layer (ligands). They are often assembled from elements of periodic groups of II-VI, III-V, or IV-VI in the periodic table. QDs have sizes below 10 nanometers and comprise energy states known as valence and conduction bands. The distance between these energy levels is called the band gap. Energy is required to excite

an electron from the valence band to the conduction band. When the excitation energy exceeds the band gap, the electron in the valence band jumps to the conduction band, leaving a hole behind in the valence band. These electron and hole pair are called exciton in their minimum energy level.

Exciton Bohr radius is defined as the physical distance between these electron-hole pair. [51]

The small size of QDs comparable with the exciton Bohr radius, causes the unique 'quantum confinement' property of these materials. [52] Quantum confinement is the leading cause for QDs having discrete band energies, size-dependent electronic and optical properties. As the size of QDs decreases, the band gap energy shifts to the higher energy as demonstrated in Figure 1.3.

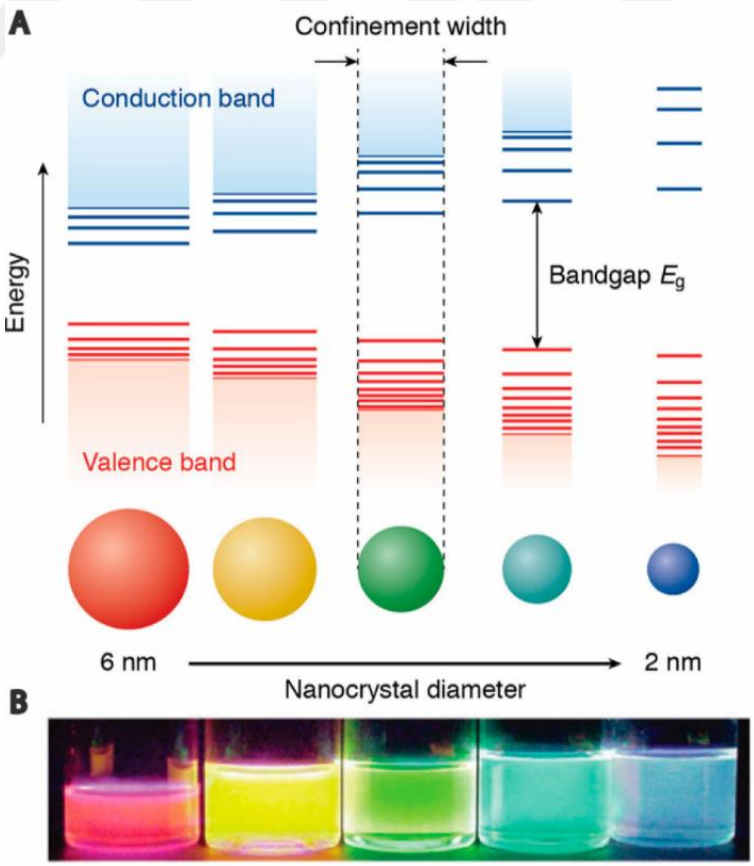

Figure 1.3. (a) The schematic representation of quantum-confinement effect in nanocrystals. (b) An example to the size-dependent emission of the QD nanocrystals under UV illumination [53].

1.5.1. Structure of Quantum Dots

QDs generally have a metalloid crystalline core, e.g. CdSe or CdTe. A bare nanocrystal core might be highly reactive, toxic, and unstable; thus, it may cause emission irregularities like 'blinking' due to surface irregularities. An inorganic shell of a different band gap semiconductor is used as a passivating layer on this core to obtain core/shell QDs. Core/shell structure is an effective approach to augment the properties of QDs. Core/shell structures have prolonged lifetimes, better chemical, physical and optical stabilities, and also reduced number of the surface traps. [54] The latter prevents the undesired charge carrier recombination. [54] By appropriate modification of the compositions of core and shell materials, band alignment and confinement potential of the quantum dots can be adjusted.

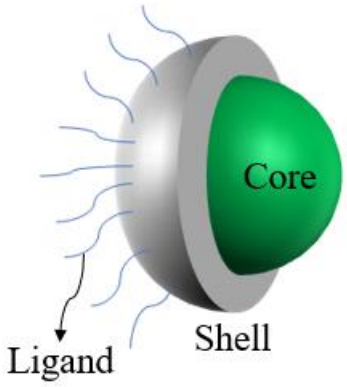

Figure 1.4. Schematic representation of a quantum dot particle covered with a passivating inorganic shell and an organic ligand.

1.5.2. Band Alignment of Core/Shell QDs and Alloy QDs

Core/Shell QDs can be classified according to the nature of bandgaps and the relative alignment of the valence band (VB) and conduction band (CB) energy levels on their core and shell materials. If the bandgap of the shell is greater than that of the core, electron and hole charge carriers are confined in the core region. This type of structure is known as type-I QDs. If either CB edge or VB edge of the shell is located in the bandgap of the core, the band alignment of these edges creates partial separation of the holes and electrons. As a result of this separation, electron and hole charge carriers are located on the different semiconductors. This type of structure is known as type-II QDs. Moreover, some quantum dots can have quasi type-II structure if the energy levels of core and shell materials are close to each other. In this structure, one type of charge carrier is located inside the core, whereas the other one is delocalized over the entire core/shell structure. (Figure 1.5.) [54] Band gaps can also be tuned by changing the compositions of QDs such as changing the ratio of S and Se in designing the alloyed CdS_xSe_{1-x} [55] nanocrystals. This capability to tune the band gaps enables the utilization of a single material for various purposes.

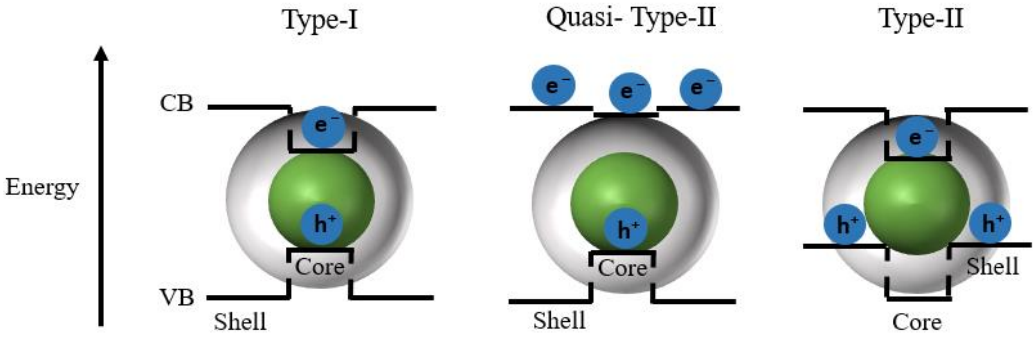

Figure 1.5. The schematic illustration of the positions of charge carriers, conduction band energies and valence band energies in type-I, quasi-type-II and type-II core/shell QD heterostructures.

1.5.3. Ligand effect

The core or core/shell structure of QDs is covered by an organic surface ligand. Ligands prevent aggregation of QDs and provide colloidal stability by forming a protective layer on the surface. The ligand selection is critical in synthesizing QDs with narrow size distribution and precise control over their shape. The bonding mechanism between ligands and QDs has similarities with molecular-scale coordination bonds found in metal complexes [56] and self-assembled monolayers on larger metal surfaces [57]. Ligands can selectively bind to the surface atoms of QDs and alter the interface energies. They can be used to modulate the physical and electronic properties of the metal atoms and determine the interactions of QDs with the surrounding solvent or matrix.

CdSe nanocrystals have become a subject of intensive study in ligand chemistry and are commonly synthesized through colloidal methods using various organic ligands. Suitable ligands for CdSe, such as carboxylic acids (e.g., oleic acid), long-chain amines, and phosphines, have enabled remarkable control of the structural properties of QDs.

[58] Ligand exchange procedures are applied to introduce new properties to the surface, which are important especially for solar cell applications of QDs.

1.5.4. Historical background

In 1982, Professor Louis Brus prepared colloidal semiconductor QDs. [59] Brus demonstrated that the optical properties of the nanoparticles in the liquid solutions were distinctly influenced by quantum size effects, which became a fundamental building block in the field of nanoscience. [60] Fluorescent QDs have found great potential in the field of electronics, particularly in photonics. The use of QDs in photonics was first found by Rocksby in 1932 when he showed that the red or yellow color of some silicate glasses could be attributed to microscopic inclusions of CdSe and CdS. [61]

In 1985, Ekimov and colleagues discovered that the changes in color observed were due to the energy states determined by quantum-confinement in CdSe or CdS QDs. [62]

In 1993, Weller provided the first comprehensive explanation of the quantum-confinement effects exhibited by colloidal semiconductor Q-particles. [63] In the same year, Murray and colleagues introduced a novel, reproducible methodology for synthesizing nanocrystals with high-quality. [64]

In the initial stages of research in this field, QDs without surface-covering shells exhibited inadequate photoluminescence (PL) and stability, which is attributed to their higher surface area-to-volume ratio compared to their bulk counterparts. Their PL quantum yield (QY) and stability were greatly improved by introducing core/shell heterostructures to protect the core surfaces from degrading environments as described above.

Placing an intermediate shell helped to relieve interfacial stress caused by a significant lattice mismatch between the core and outer shell of the heterostructured QD. [65] Thus,

provided outstanding PL characteristics such as ultra-high QY. These enhanced PL characteristics lead these shelled QDs to be used in several application fields, especially in optoelectronic devices, as they can replace the bulk phosphors used in LEDs. Different compositions of phosphors were used in conventional LEDs to generate different colors, whereas current QD-LEDs enabled the realization of all colors in the visible region with the same composition of materials with only varying particle sizes. Also, the narrower emission bandwidth of QDs allowed QD-based displays to achieve a wider color gamut than organic emissive materials. Hence, shelled QDs have been adopted as color converters in commercial displays. Electroluminescent (EL) type QD light emitting diodes (QLEDs) are widely studied as the next generation of display technology. Utilization of QDs in photovoltaic devices such as solar cells and photodetectors [66], for which absorption abilities of materials in a specific spectral range are needed, also emerged as an important application field of QDs. [65]

1.5.5. Synthesis of Quantum Dots

Development of various synthesis methods to control size-dependent properties of the QDs led to advancements in the wide range of application fields for these nanoparticles. Top-down and bottom-up techniques are used in synthesizing QDs.

1.5.5.1. Top-Down Approaches

In the top-down approaches, a bulk semiconductor is thinned to form the QDs. These synthesis methods involve beam lithography, reactive-ion etching, focused beam lithography, and dip-pen lithography. These methods provide precise control over the shape, size, and configurations of quantum dots. However, these methods have some limitations, such as the potential incorporation of impurities into the quantum dots and the introduction of structural imperfections during the patterning stages. [67]

1.5.5.2. Bottom-Up Approaches

Bottom-up approaches in synthesizing QDs involve the various physical and chemical methods to form the nanoparticles. This method typically starts with the controlled growth of the semiconductor materials at the nanoscale level. The colloidal synthesis technique is commonly utilized to achieve this controlled growth.

1.5.5.2.1. Colloidal synthesis

The most common method to synthesize QDs is the colloidal synthesis, which chemically produces the QDs as a suspension. In colloidal synthesis, the QD formation includes the nucleation and the growth process. This synthesis starts with the injection of the precursor material into the solvent. Then the reaction is heated to enable the QD growth. First, a supersaturated solution is obtained, which nucleates to produce small nanocrystals. Both kinetics and thermodynamics contribute to the nanocrystal growth. By tuning the pH, temperature, and reaction time length, the final size of the QDs can be controlled [68].

1.6. Carbon Dots (CDs)

Carbon dots (CDs) are naturally fluorescent nanoparticles having a few nanometers in size range. It was first synthesized by Xu et al. accidentally during the purification of single-walled carbon nanotubes (SWCNT) in 2004. The name "carbon dots" was first introduced in 2006 by Sun and coworkers. [69] They synthesized fluorescent CDs with quantum confinement effect by laser ablation in the presence of water vapor with argon as carrier gas.

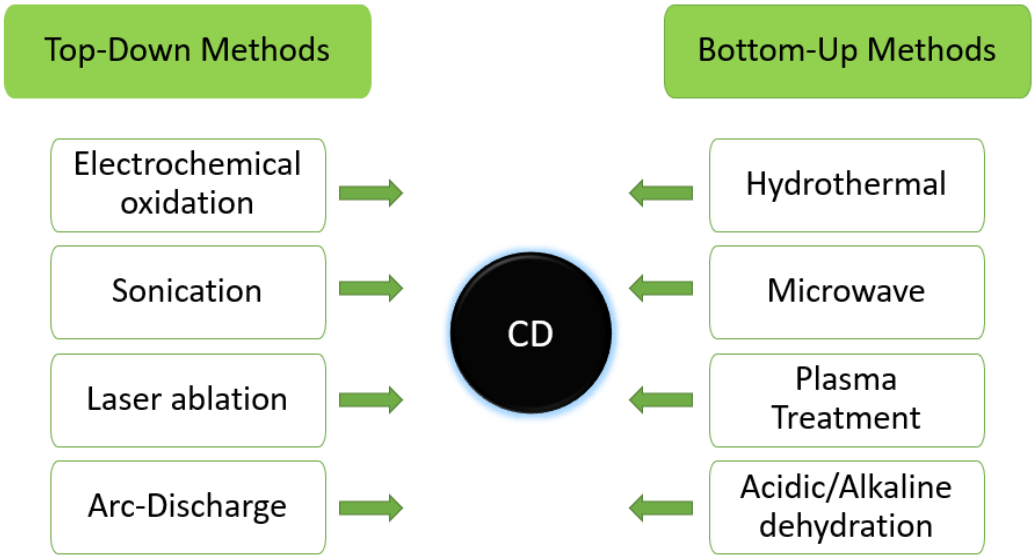

Figure 1.6. Schematic illustration of top-down and bottom-up approaches for carbon dot synthesis

Following the laser ablation method, several ways to synthesize fluorescent carbon dots have been developed. [70]–[72] However, most of these synthesis methods need several steps and the synthesized carbon dots suffer from very low photoluminescent quantum yields (QY). Then, a novel one-step hydrothermal/solvothermal strategy to synthesize carbon dots was first introduced in 2010. This method utilizes the carbonization process of carbon precursors in a hot non-coordinating solvent. CDs synthesized by the hydrothermal method have several functional groups on their surfaces, such as carbonyl, hydroxyl, and carboxyl groups that give the carbon nanoparticles ability to be soluble in water. [73] The hydrothermal method allowed a wide range of precursors to be used in obtaining CDs, such as glucose, citric acid, coffee powder, amino acids and biomass waste. Given their ability to be soluble in water, green precursors and environmentally friendly synthesis methods, carbon dots have been shown to have better biocompatibility and lower toxicity compared to common organic dyes. [73] Therefore, carbon dots have been mainly used in applications such as bioimaging, biomedicine and drug delivery. [74] The hydrothermal method also allowed the

introduction of heteroatoms, e.g., boron (B) and nitrogen (N), to the carbon structure in the synthetic steps. Introducing heteroatoms to carbon dots significantly extended their applications by enhancing their photoluminescence and stability. Further, it enabled a better control over their emission wavelengths. [75]

1.6.1. Nitrogen-Doped Carbon Dots (N-CDs)

Doping the carbon dots with nitrogen is reported to increase their quantum yield remarkably. Compared to undoped CDs, the relative content of oxygen-containing functional groups decreases with the addition of nitrogen. Nitrogen doping leads the surface to be modified by the addition of nitrogen-containing groups like amides and amines. The formation of nitrogen-containing surface centers is the reason behind the increased quantum yield. Imide rings fused to the carbogenic core are the potential structures for green-range emission.

N-CDs are commonly prepared through the hydrothermal method. This process involves heating nitrogen-containing carbon precursors in an aqueous solution under high temperatures in an autoclave. High temperature and pressure inside the autoclave initiate the carbonization (pyrolysis) and favors the in-situ nitrogen doping of carbon dots. Reaction temperature and time significantly affect the quantum yield of the obtained N-CDs. [76] Using a single precursor as a carbon and nitrogen source, such as a protein or an amino acid renders the synthetic method a low-cost and straightforward process.

1.7. Poly (dimethyl siloxane)

Poly (dimethyl siloxane) or PDMS is a non-toxic and optically clear silicon-based organic polymer. It comprises an inorganic backbone with alternating silicon (Si) and oxygen (O) atoms with two methyl groups attached to the Si. PDMS demonstrates outstanding chemical and thermal stability due to the Pauling electronegativity difference of 1.7 between Si and O. This electronegativity difference results in an increased dissociation energy (445 kJ/mol). The bonding angle of Si-O-Si bonds in PDMS is 143°, allowing an easy backbone rearrangement of methyl groups at the surface and interfaces. [77] This easy rearrangement provides PDMS mechanical flexibility. Furthermore, PDMS has a low surface free energy that conveys hydrophobicity to the polymer. This low surface energy depends on molar mass and closely bonded methyl groups. The covalent nature of Si-O and Si-C bonds allows PDMS to fragment into radicals quickly. The radicals created on PDMS as a result of a mechanical input (mechanoradicals) can be detected quantitatively and qualitatively [11]. Since the Si-O bonds are polar, the mechanical input can also lead to heterolytic cleavage and the formation of mechanoions [78] which are abundant enough to drive chemical reactions on the surface of the polymer. The efficient formation of the mechanospecies on its surface that decay in a moderate rate and the flat, conformal casting of the polymer of flat surfaces that enables the very low surface roughness (ideal for contact electirification studies) make PDMS an easy-to-work-with material in contact electrification studies [79]–[81] We should note that the material used in these studies is the crosslinked PDMS – not the linear PDMS. The crosslinked material is typically formed using the commercial kit containing the prepolymer base and the curing agent mixed at a common ratio of 10:1 (v/v). The crosslinked material is shortly referred in the literature as ‘PDMS’, too. The bulk properties of the crosslinked PDMS,

such as its mechanical strength and visible light transparency, can be modified by changing the mixing ratios of base and curing agent and/or reaction conditions. For example, an increase in stiffness can be expected if 5:1 ratio of the prepolymer base and the curing agent instead of a 10:1 ratio. Stiffness is an essential factor in the context of the generation of static charges through contact and separation of materials.

1.8. Thermoplastic Polymers

Thermoplastic polymers are a group of materials that can have reversible transitions between their solid state and molten state. They are softened and can be melted upon heating and resolidifies upon cooling. This specific property distinguishes them from thermoset polymers that undergo irreversible curing processes. Thermoplastic polymer properties such as mechanical strength, melting point, ductility etc. are easily tuned by changing their composition and molecular structure. They have reshaped many industries with their tunable properties and easy processing. Almost 450 million metric tons of thermoplastics are projected to be produced globally in 2025. [82] For instance, polystyrene (PS) is used in plastic parts of cars and packaging, polyethylene (PE) is used in pipes or durable goods, polymethyl methacrylate (PMMA) is used in optical applications due to its excellent light transmission properties, and polyvinyl alcohol (PVA) is used in adhesives and textile industry. The examples of thermoplastics are numerous. In this thesis we studied the QD composites of PE, PS, PMMA, and PVA (Figure 1.7). These polymers were selected because 1) PE and PS are among the most produced thermoplastics and they differ a lot in their chemical structure (one has no pendant group and the other has a large aromatic group, which may act differently upon charging) 2) PMMA and PVA are used frequently in triboelectric generators. We have

selected ‘moderate’ molecular weights and the commercial chemical products of linear polymers to keep this study at the basic level. (See Section 2.1.)

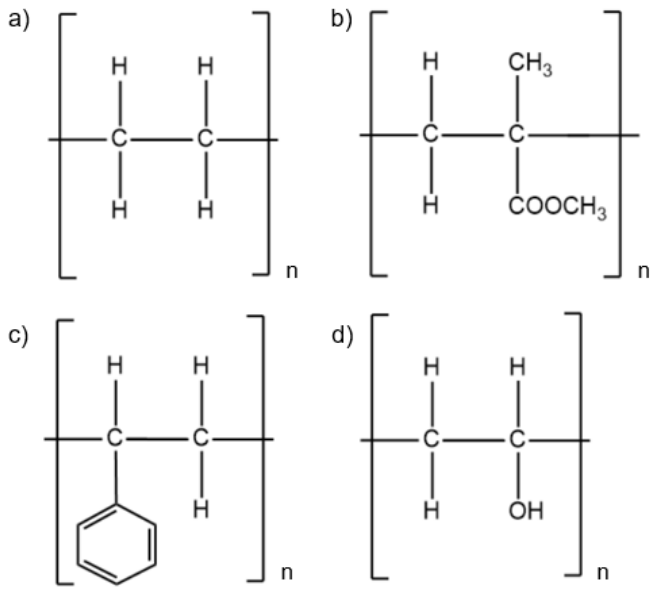

Figure 1.7. Molecular structure of thermoplastic polymers a) polyethylene b) poly (methyl methacrylate) c) polystyrene d) polyvinyl alcohol

1.9. Aim of the Thesis

Controlling and manipulating the contact charges is essential in solving problems caused by uncontrolled electrostatic discharge and effectively using contact charges in useful applications.

Our group recently has shown that introducing organic dyes and organic charge transfer complexes into the polymers can lead polymers to attain antistatic properties. The mechanism behind such an antistatic behavior is the electronic interaction of mechanospecies with the additives in the polymer leading to fast discharging. It was also shown that this antistatic effect could further be manipulated by illuminating the doped polymer with UV light that excited the dopant. In our previous study, we used some organic charge transfer complexes of different donor and acceptor molecules to tune HOMO-LUMO band gaps of the dopant materials. [45] We showed that it is possible to affect the discharging efficiency by the tuning of the bandgap of the dopant. The success of this approach led us to think that the same bandgap engineering approach might be used with QDs as dopants in polymers, to enhance the contact charge stabilization or foster the charge mitigation on polymers. Thanks to their unique quantum confinement effect, quantum dots have versatile band-gap tunability as explained above. The physical distribution of charge carriers in the nanostructure can also be manipulated by light, which can provide an additional control over their interaction with the mechanospecies in the polymer. QDs have high photostability compared to the organic dyes and organic charge transfer complexes. We first formed an elementary polymer composite system with PDMS (the benchmark material of contact electrification studies) and the three types of the QDs, type I, type II, and quasi type II. [83]-[84] The results of the contact charging and charge decay experiments in

this study showed that the proof-of-principle of the QD/mechanospecies interactions. They also displayed that various types of QD can affect the charge/discharge differently and also there is a significant effect of illumination on the charging/discharging rates of the QD-PMDS composites. Encouraged by this observation, this thesis aimed to investigate the QD-polymer interactions by testing different heterostructures and surface chemistries of QDs, the efficiency of the interaction in composites of different polymers. The first-time investigation of such a QD/thermoplastic mechanoradicals interaction can help to probe the QDs as potential antistatic dopant or charge enhancers in the thermoplastics, which are not only used in various current industries (electronics, packaging, air and space etc.) but also utilized in the emerging ones like triboelectric generators.

Chapter 2

2. EXPERIMENTAL METHODS AND MATERIALS

2.1. Materials

PDMS samples were prepared by using a Dow Corning Sylgard 184 silicone elastomer kit.

All solvents were anhydrous and were used as received without further purification. Hexane (99%, Aldrich), Toluene (99%, Aldrich). Bovine Serum Albumin (BSA), PMMA (Mw: 350000), and PE (Mw: 4000) were purchased from Sigma Aldrich. PS was obtained from ISOLAB sterile polystyrene petri dishes. Polyvinyl alcohol was purchased from Aromel Kimya Medikal A.Ş. 0.22 μm PTFE syringe filter membrane was purchased from ISOLAB. The PPL-Lined hydrothermal reactor was purchased from Kent Kimya. Aluminum stubs (Agar Scientific) were used to mount the samples for contact charge measurements in the homemade tapping device explained below.

2.2. Synthesis of Inorganic Quantum Dots

Synthesis of inorganic quantum dots was done by Ms. Firdevs Aydın from METU Chemistry Department.

2.3. Synthesis of N-CDs

Nitrogen-doped carbon dots are synthesized via hydrothermal process using aqueous Bovine Serum Albumin (BSA) solution in accordance with the literature method. [85] 0.2 g of BSA was added to 20 mL of ultrapure water and stirred for 15 min at room temperature to prepare a homogeneous solution. This solution was transferred to a 50 mL PPL autoclave and heated at 200°C for six hours in a hot air oven. After cooling to

room temperature, the carbide slag was removed from the product solution via centrifugation at 10 000 rpm for 15 min. The yellow-brown solution obtained was then filtrated by using a 0.22 µm pore size Millex® PVDF syringe filter. The final solution was analyzed by various characterization methods. An illustration of the synthesis method is given in Figure 2.1.

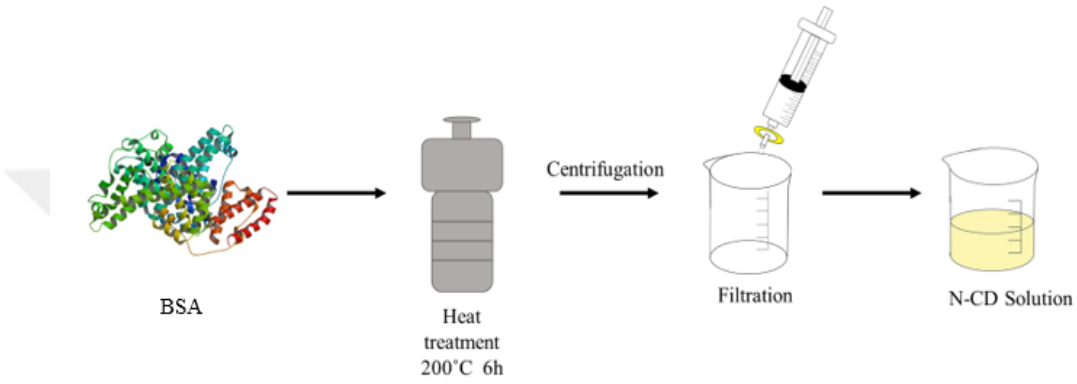

Figure 2.1. Schematic illustration of synthesis method for N-CDs.

2.4. QD Doping to PDMS

QDs having different heterostructures were doped into PDMS polymer by in-situ polymerization method. PDMS was prepared using a Dow Corning Sylgard 184 silicone elastomer kit with a ratio of 10:1, base polymer, and curing agent. The mixture of the prepolymer was stirred and mixed for 15 minutes. The QD solution of 4.0 mg/mL was added during mixing. After obtaining homogeneity, the mixture was poured into the polystyrene dishes (providing the flat surface) for curing. The mixture was kept under vacuum for degassing the air bubbles formed during mixing. Curing was completed in 24 hours at 70˚C in the oven. Then the pieces are cut into discs, each having a diameter of 1.7 cm.

2.5. Preparation of Type-I QDs-PS Composites

Nanocomposites of PS were prepared by vigorously stirring the QD solution in hexane with the PS polymer solution. 1.0 g of PS was dissolved in 10 mL toluene and left for overnight mixing. After a homogeneous polymer solution was obtained, 0.3 mL of QD solution (5.0 mg/mL) in hexane was added to 0.7 mL of polymer solution and stirred for an hour to obtain homogeneous mixing. Control samples are prepared under the same conditions with the with addition of 0.3 mL pure hexane to the polymer solution. The prepared composite solutions were used to coat 18x18 mm glass substrates by dip coating method. The solvent was evaporated under the vacuum at ambient temperature.

2.6. Preparation of Quasi-Type-II QDs-Polymer Composites

Nanocomposites of PS, PE, and PMMA were prepared through the vigorous stirring of the solution of QDs in hexane at varying concentrations (2.0 mg/mL, 4.0 mg/mL, 6.0 mg/mL, and 8.0 mg/mL) in polymer solutions. 1.0 g of PS, PE, and PMMA polymers were dissolved in 10 mL toluene and left for overnight mixing.

After homogeneous polymer solutions were obtained, 0.3 mL of QD solution in hexane was added to 0.7 mL of polymer solution and stirred for another hour to obtain homogeneous mixing. Control samples are prepared in the same conditions.

The prepared composite solutions were used to coat 18x18 mm glass substrates (each glass substrate is coated with 0.1 mL of mixture solution) by spin coating method at 1500 rpm for 30 s. The solvent was evaporated under the vacuum at ambient temperature.

2.7. Preparation of N-Carbon Dot-PVA Composites

N-CD-PVA composites were prepared according to the method modified from the literature. [86] 0.25 g of PVA was added to 5 mL of water and continuously stirred at 80˚C for 5 hours to obtain a homogeneous transparent aqueous solution. The solution was cooled to room temperature. After a homogeneous polymer solution was obtained, aqueous N-CD solution in water was added in different volume ratios of PVA:N-CD solution (1:0.25, 1:0.5, and 1:1) and stirred for another hour to obtain homogeneous mixing. Control samples are prepared under the same conditions. The prepared composite solutions were used to coat 18x18 mm glass substrates by spin coating method (each glass substrate is coated with 0.1 mL of mixture solution) at 1500 rpm and for 30 seconds. The solvent was then evaporated under the vacuum at ambient temperature, and N-CD-PVA composites were obtained.

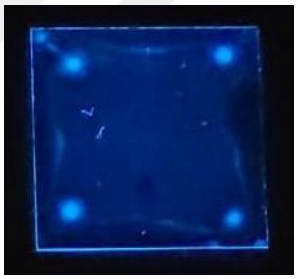

Figure 2.2. The photo of N-CD-PVA composite coated on glass under 364 nm UV illumination

2.8. Characterizations

Chemical, optical, and structural properties of materials used in this thesis work were characterized by using UV-Visible Spectroscopy (UV-VIS), Fluorescence Spectroscopy, X-Ray Diffraction (XRD), Atomic Force Microscopy (AFM), Time-Resolved Fluorescence (TRF), Transmission Electron Microscopy (TEM), Energy-

dispersive X-ray Spectroscopy (EDX). In addition, the conductivities of solid samples were measured by the two-probe method using an electrometer.

2.8.1. UV-Visible Spectroscopy (UV-VIS)

The absorption spectra were recorded using a UV-Vis-NIR Spectrophotometer (Cary 5000) by Agilent. A baseline measurement was initially made using a reference material (e.g., the solvent of the solutions) to record the background absorption. Then, the sample was placed in the sample holder against the reference, and UV-Vis spectra were obtained over the desired wavelength range (usually from 200 nm to 800 nm) with a 600 nm/min scan rate and in the double beam mode.

2.8.2. Fluorescence Spectroscopy and Time-Resolved Fluorescence (TRF)

The emission spectra were recorded using TRF spectroscopy using either 3 nm or 5 nm side entrance and exit slits with an integration time of 0.1 s.

Time-correlated single photon counting (TCSPC) was used to record luminescence lifetime decays of QD solutions by the same spectrophotometer. The instrument response function (prompt) was collected by using 1 or 2 droplets of LUDOX solution in distilled water to arrange the α value, which counts the percentage of photons coming from the sample.

2.8.3. X-Ray Diffraction (XRD) Analysis

The crystallographic structure of QD solutions was recorded using the X'Pert PRO, PANalytical model X-ray diffractometer with Cu Kα radiation. 40 mA current and 45 kV accelerating voltage was applied. The Cu Kα radiation has a wavelength of 1.5406

Å. The QD solution was drop-cast on a silicon wafer and then placed in the XRD device sample holder.

X-Ray Diffraction Analysis of N-CD powder was recorded in the Materials Science (MS) beam-line at SESAME (Synchrotron-light for Experimental Science and Applications in the Middle East). N-CD aqueous solution obtained after the synthesis was lyophilized and inserted into a capillary tube. The synchrotron X-Ray has a wavelength of 0.82745 Å.

2.8.4. Energy-Dispersive X-ray Spectroscopy (EDX)

The EDX analysis of samples was performed with a Quanta 200F model SEM embedded with an energy-dispersive X-ray spectroscopy (EDX) detector. The spectra were obtained under an accelerating voltage of 15 kV for polymer samples.

2.8.5. Atomic Force Microscopy (AFM)

The roughness analysis was made using atomic force microscopy (AFM) by Oxford Instruments in tapping mode. Imaging was done over a 5.0 μm × 5.0 μm scan size.

2.8.6. Transmission Electron Microscope (TEM)

Samples for the TEM imaging were prepared by drop-casting dilute solutions of QDs and N-CDs onto 200 Mesh carbon-coated copper transmission electron microscope (TEM) grids. TEM images were taken using JEOL TEM 2100F (200 kV) embedded with an energy-dispersive X-ray spectroscopy (EDX) detector. Image J software was used for the determination of particle size distribution plots.

2.8.7. FTIR-ATR

The functional groups of the QDs in solutions were analyzed using the Bruker Alpha FTIR-ATR Spectrometer. All samples were analyzed with 64 scans with 4 cm^{-1} resolution. The spectra obtained were baseline corrected.

2.8.8. Lyophilizer

Lyophilization of synthesized N-CDs was completed using a 4.5 L freeze dryer system by Labconco. The aqueous solution of N-CD was cooled using liquid nitrogen and placed in a freeze-dryer. After three days, the powder of N-CD was obtained.

2.8.9. Electrical Measurements

2.8.9.1. Measurement of generated contact charge

Contact charging of samples was monitored by using a homemade tapping device that is connected to an oscilloscope. A two-channel oscilloscope was used to measure the open circuit electrical potential (in volts) generated during the contact and separation of the two counter surfaces, which are connected to two electrode probes. Samples were mounted on aluminum stubs with carbon tape connected to a 100 megaohm (input impedance) oscilloscope probe. The second surface (aluminum or PTFE) was mounted on another metal stub attached to an identical probe. As the surfaces are contacted and separated, charge generation and accumulation took place. These accumulated charges developed a positive or negative potential and these potentials were recorded by the oscilloscope when charges were at their maximum values. 1 Hz tapping frequency was used. The electric potential generated upon tapping the thermoplastic polymers against

PTFE and Al was recorded in V_{oc} (mV). Tapping measurements were done in dark and under UV illumination. Schematic representation of the tapping device is given in Figure 2.3.

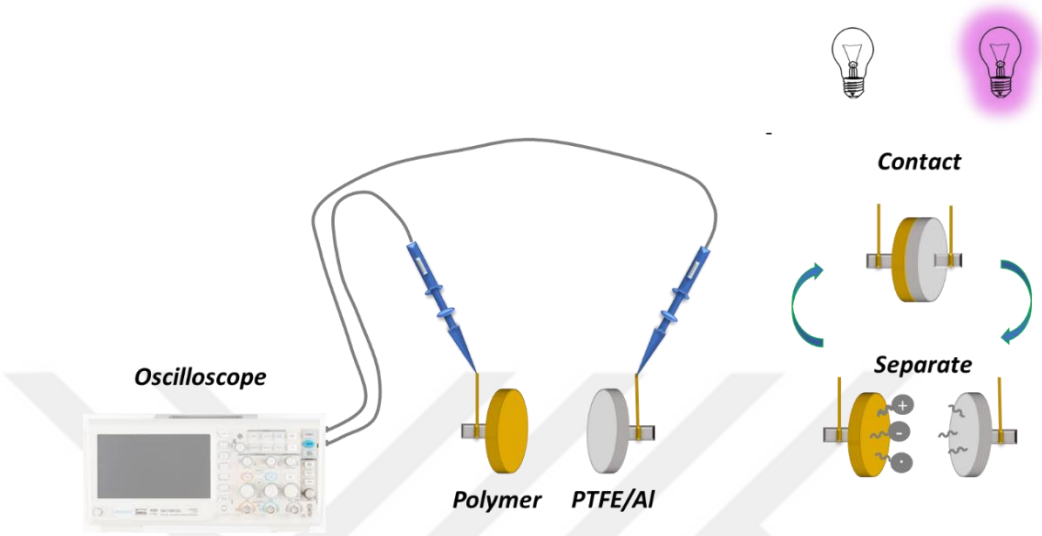

Figure 2.3. Schematic illustration of the tapping device and the contact charge generation measurements.

2.8.9.2. Measurement of the charge mitigation

QD-doped PDMS polymers were contact charged against aluminum foil up to -1.7 nC. Then they were immersed inside a Faraday cup which is connected to an electrometer. The net charge on the polymer is measured by the Keithley electrometer (6514) and recorded using Kickstart software. Charge stability in the cup was recorded for 20 minutes for each sample in dark and under UV illumination. Figure 2.4. shows a schematic representation of the setup for charge stability measurements.

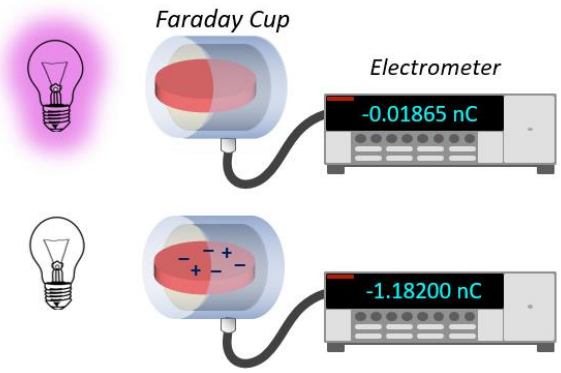

Figure 2.4. Schematic illustration of charge stability measurement setup. Charge stability can be measured with this setup in dark, or under illumination with a light source (which is a UV lamp in this study).

2.8.3. Surface Conductivity Measurements

Surface resistivities of QD doped polymer and undoped polymer were measured using a two-probe method, with w = 18 mm wide samples, and the distance between electrodes (d) is 217 μm. Resistances, R, were collected by Keithley electrometer (6517B), which served as the voltage source using a two-wire resistance measurement setting. 100 V is applied for 3 samples in each group. From the resistance measurement, the values were calculated for surface conductivity, ƙ, according to equation ƙ = 1/ρ , p= R x (w/d).

Chapter 3

3. RESULTS AND DISCUSSION

This thesis aims at discovering the effect of the QD doping in the contact charging of PDMS and some thermoplastic polymers. In detail, the effect dopant QD electronic structure in contact charge stability of PDMS and thermoplastic polymer QD composites was studied.

Firstly, we investigated the effect of charge carrier locations on various QDs on contact charge stability of PDMS polymer. PDMS prepolymer can be cured flat on surfaces, preventing errors from the different roughness samples. Therefore, PDMS polymer was chosen for this study. Previously, it was shown that the core/shell QDs affect the charge stability differently according to their types, type-I, type-II, and quasi type-I. [84] Here, we doped alloy QDs having different elemental ratios in PDMS and analyzed the composites' charge mitigation to compare it with the core/shell QDs.

Then, using the homemade tapping setup, the charge generation propensities of the thermoplastics were recorded. Using the tapping setup rather than the charge decay setup has more advantages for thermoplastic polymers because it is hard to prepare thermoplastic polymer samples as thick, homogenous pieces to be used in charge decay measurements.

After the alloy QDs study, the effect of the QD ligand in the charging of the composite was investigated by doping type-I CdSe/ZnSe into polystyrene polymer.

Next, we doped quasi-type-II CdSe/ZnSe QDs to three different thermoplastic polymer matrices to understand the variations in contact charging for different polymers.

In the final part of the thesis, the charge generation of PVA - a biodegradable thermoplastic polymer was investigated with and without doping with nitrogen-doped carbon dots.

In all parts, contact charge stability on QD composites were compared to those of pristine polymers in dark and under UV illumination.

3.1. Contact Charge Stability on CdS_xSe_{1-x}/ZnSe doped PDMS

In this part of the work, we doped CdS_xSe_{1-x} and the CdS_xSe_{1-x}/ZnSe QDs with different S to Se ratios to probe the effect of the change in the bandgap of QDs on the contact electrification of the composites. We prepared CdS, CdSe, $CdS_{0.4}Se_{0.6}$, $CdS_{0.4}Se_{0.6}$/ZnSe, $CdS_{0.6}Se_{0.4}$, $CdS_{0.6}Se_{0.4}$/ZnSe, CdSe/ZnSe (type-I) and CdS/ZnSe (type-II) QDs and doped them into PDMS polymer, as explained in the experimental section. Then we recorded the charge stability of the composites in dark and under UV illumination, as detailed below.

3.1.1. Preparation and Characterization of the Quantum Dots

Table 3.1. The maximum absorption and emission wavelengths of the prepared QD solutions*

QD	Absorption ʎ max	Emission ʎ max	Quantum Yield
CdS	416 nm	426 nm	0.9%
CdSe	570 nm	576 nm	1.1%
$CdS_{0.4}CdSe_{0.6}$	488 nm	528 nm	1.86%
$CdS_{0.4}CdSe_{0.6}$/ZnSe	556 nm	576 nm	6.43%
$CdS_{0.6}CdSe_{0.4}$	458 nm	482 nm	0.99%
$CdS_{0.6}CdSe_{0.4}$/ZnSe	526 nm	553 nm	29.20%
CdSe/ZnSe (Type-I)	592 nm	611 nm	44.50%
CdS/ZnSe (Type-II)	-	525 nm	36.30%

*Measured and calculated by Ms. Firdevs Aydın

TEM images of core $CdS_{0.6}Se_{0.4}$ and core/shell $CdS_{0.6}Se_{0.4}$/ZnSe are given in Figure 3.1. As a result of TEM analysis, particle size and size distribution of the $CdS_{0.6}Se_{0.4}$ core were calculated as 3.1 ± 0.4 nm and 12.8 %, respectively. Size and size distribution of the $CdS_{0.6}Se_{0.4}$/ZnSe QDs were calculated as 6.9 ± 0.8 nm and 11.7 %, respectively by using Image J program. Size and size distributions are calculated by Ms. Firdevs Aydın.

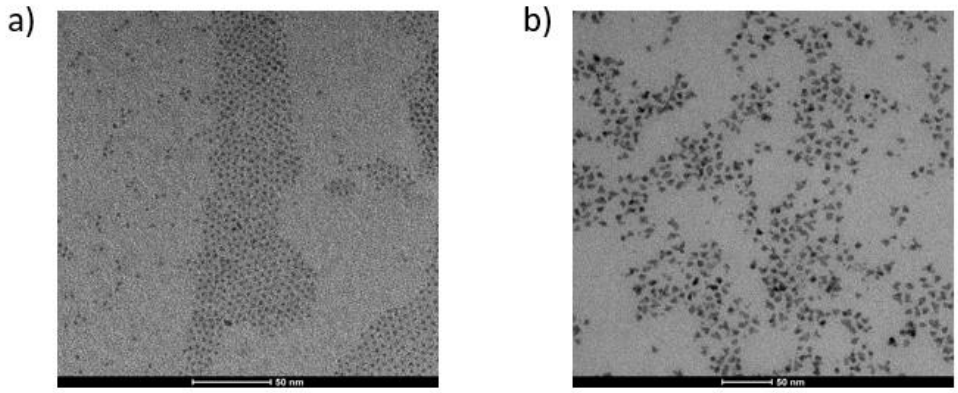

Figure 3.1. TEM images of a) $CdS_{0.6}Se_{0.4}$ b) $CdS_{0.6}Se_{0.4}$/ZnSe QDs

3.1.2. Preparation and Characterization of the QD-doped PDMS

QD-doped PDMS polymers were prepared as described in section 2.4. by in-situ polymerization method. The absorbance graph of QD-doped polymers is given in Figure 3.2.

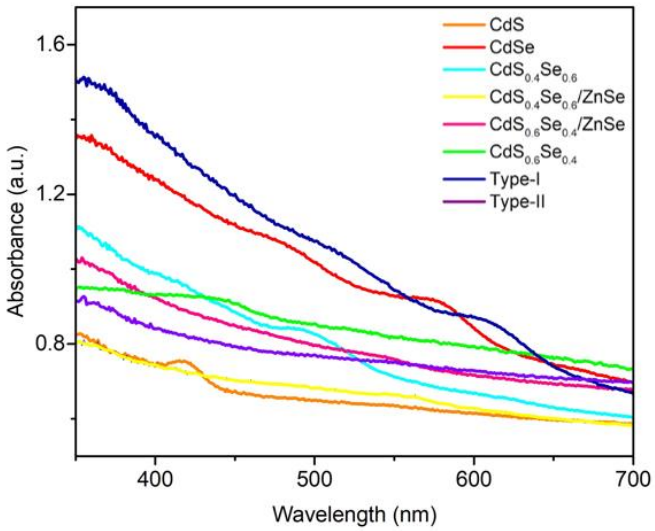

Figure 3.2. The UV-Vis absorbance spectra of the QD-doped PDMS.

3.1.3. Charge Decay Experiments of PDMS

QD-doped PDMS polymers were contact-charged against aluminum foil up to -1.7 nC. Then, the samples were immersed and kept in the Faraday cup, and the charge was left to decay in the air. The charge versus time data (Figure 3.3) were obtained by repeating the procedure in the dark and under UV illumination for all samples, and the decay rate constants were calculated using this data. Decay profiles of QD-PDMS composites were analyzed using both first and second-order reaction kinetics. For first-order reactions, the linear plot of ln [charge] versus time has a slope of -k, where k is the rate constant. For second-order reactions, the linear plot of 1/[charge] versus time gives a slope equal to k. These k values are calculated using the first and second-order plots for all alloy QDs. The resulting decay rate constants of the composites are given in Table 3.2. Standard deviations were calculated from four independent measurements. Relative humidity during the measurements was recorded as 20%-21%.

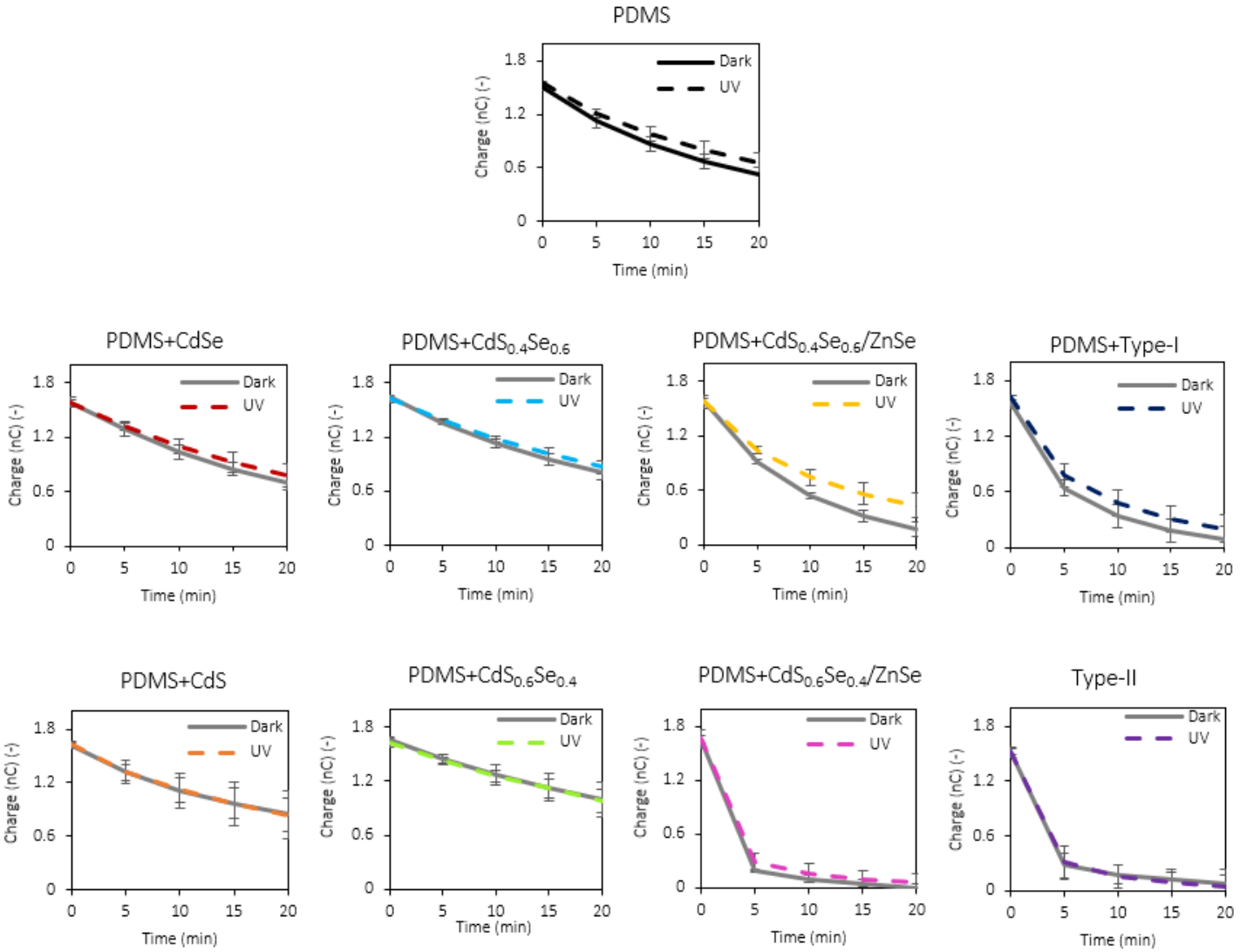

Figure 3.3. Charge versus time data for PDMS composites of QDs with different heterostructures.

Table 3.2. The decay rate constants of contact charges on the QD-doped PDMS samples 5 minutes after contact charging and corresponding R^2 values of the first and second order plots.

Sample	First order rate constant (s^{-1})	R^2	Second order rate constant ($charge^{-1}\ s^{-1}$)	R^2
PDMS-Dark	0.06±0.01	0.98	0.05± 0.01	0.99
PDMS-UV	0.05±0.01	0.99	0.04±0.01	0.99
CdS-Dark	0.04±0.02	0.99	0.03±0.01	0.99
CdS-UV	0.04±0.01	0.99	0.03±0.01	0.99
CdSe-Dark	0.04±0.01	0.98	0.03±0.01	0.99
CdSe-UV	0.04±0.01	0.99	0.02±0.01	0.99
$CdS_{0.4}Se_{0.6}$-Dark	0.04±0.00	0.98	0.02±0.00	0.99
$CdS_{0.4}Se_{0.6}$-UV	0.03±0.00	0.99	0.02±0.00	0.99
$CdS_{0.4}Se_{0.6}$/ZnSe-Dark	0.10±0.02	0.99	0.09±0.01	0.99
$CdS_{0.4}Se_{0.6}$/ZnSe-UV	0.08±0.01	0.99	0.07±0.01	0.99
Type-I-Dark	0.18±0.04	0.99	0.19±0.05	0.99
Type-I-UV	0.15±0.04	0.99	0.14±0.05	0.99
$CdS_{0.6}Se_{0.4}$-Dark	0.03±0.01	0.99	0.02±0.01	0.99
$CdS_{0.6}Se_{0.4}$-UV	0.03±0.01	0.99	0.02±0.00	0.99
$CdS_{0.6}Se_{0.4}$/ZnSe-Dark	0.88±0.08	0.91	0.88±0.08	0.99
$CdS_{0.6}Se_{0.4}$/ZnSe-UV	0.65±0.26	0.93	0.65±0.26	0.99
Type-II-Dark	0.79±0.46	0.90	0.79±0.46	0.98
Type-II-UV	0.84±0.69	0.91	0.84±0.69	0.99

As a result (Table 3.2.), the second order decay rate constants of $CdS_{0.6}Se_{0.4}$/ZnSe and type-II doped PDMS were calculated as 0.88 ± 0.08 $charge^{-1}\ s^{-1}$ and 0.79 ± 0.40 $charge^{-1}\ s^{-1}$ in dark, respectively. Since the first-order linear plots of these QDs have R^2 values smaller than 0.95, their rate constants are also calculated by fitting to second-order kinetics and it is shown that the decay rates of these QDs fit second-order better.

Further, if we compare with the undoped PDMS having 0.05 ± 0.01 charge^{-1} s^{-1} rate constant, the charge decay rate has dramatically increased by doping these QDs. A similar increase in decay rate was observed under UV illumination, too.

Rate constants of $CdS_{0.4}Se_{0.6}$/ZnSe and type-I doped PDMS were found as 0.09 ± 0.01 charge^{-1} s^{-1} and 0.19 ± 0.05 charge^{-1} s^{-1} in the dark, respectively. That shows a faster charge decay compared to the undoped PDMS sample with a rate constant of 0.05 ± 0.01 charge^{-1} s^{-1}. We observed that the decay rate constant is slightly slower under UV illumination for same QDs compared to dark with constants 0.07 ± 0.01 charge^{-1} s^{-1} and 0.14 ± 0.05 charge^{-1} s^{-1} respectively.

Moreover, comparing different core/shell QDs, $CdS_{0.6}Se_{0.4}$/ZnSe and type-II QD doped PDMS showed the fastest dissipation of charges on the polymer surfaces.

3.1.4. Discussions

In our previous study [84], we showed that the core QDs without shells (CdS and CdSe) have similar charge decay constants as the undoped PDMS under dark and UV illumination. The charge decay-inertness of the doped naked QDs implied that the core-shell system plays a significant role in the discharge or no-discharge process. (However, another simple explanation for this inertness can be the trap states or Auger recombination [87]. Also, naked core QDs may be oxidized easier than core/shell structures, hindering their activities after doping to the polymer.) In this work, we replicated these results to compare them with those obtained from the composites with alloy core QDs, $CdS_{0.4}Se_{0.6}$ and $CdS_{0.6}Se_{0.4}$. These core-only QDs gave similar results to the previously analyzed CdS and CdSe, showing that a core/shell structure is necessary to affect the contact charge stability on the composite.

A more significant outcome of our previous study [84] was; quasi-type-II and type-II QDs interact more efficiently with mechanospecies generated on polymers than type-I core shell QDs. This better interaction was attributed to the closer proximity of charge carriers in quasi-type-II and type-II QDs to the polymer mechanospecies - in comparison to the decreased interactions of the charge carriers confined only in the core of type-I core/shell QDs, leading to slower dissipation of charges in the type-I PDMS composites.

In this study, we prepared and probed PDMS samples with alloy core/shell QDs $CdS_{0.4}Se_{0.6}$/ZnSe and $CdS_{0.4}Se_{0.6}$/ZnSe. Among all the composites, the fastest charge decay of contact charges was observed with PDMS doped with $CdS_{0.6}Se_{0.4}$/ZnSe and type-II QDs. As evident from the results of charge decay rate calculations, the increase in the S to Se ratio in QDs is particularly important to affect a faster charge decay. The decay kinetics of PDMS doped with $CdS_{0.6}Se_{0.4}$/ZnSe is similar to those obtained with PDMS doped with quasi-type-II and type-II QDs. As the S/Se ratio increases the band alignment of the alloy core shell particle gets similar to those of the core/shell quasi-type-II and type-II QDs. On the other hand, as the S/Se ratio decreases, the QD band structure resembles that of type-I QDs, and a slower charge decay is observed, which is further slightly slower under UV since the excitons are all located in the core in the excited QD. (UV illumination did not affect the decay rates of the composites with quasi-type-II, type-II QDs, or $CdS_{0.6}Se_{0.4}$/ZnSe.)

In summary, the results with the naked alloy core and alloy core/shell QDs are in line with our previous hypothesis on ‘the location-dependent interaction of charge carriers on QDs with contact charges’ on the PDMS surface.

3.2. Ligand Exchange with Pyridine in Quantum Dots in Charge Generation

UV-Vis absorbance, photoluminescence, and FTIR spectra were taken and quantum yield of the QDs, and size distribution of the QDs were calculated by Ms. Firdevs Aydın. Lifetime measurements were taken by Ms. Sunay Dilara Ekim.

Ligands are the covering organic molecules on the surface of the QDs. Long carbon chains of ligands can form a barrier to charge carriers, passivate the surface and change the solubility properties of QDs. Therefore, surface ligand engineering of the QDs is critical, especially for the applications of QD-polymer nanocomposites. [88]

In this part of the work, we investigated how changing the ligands in QDs affects the charge generation properties of the QD-PS nanocomposites. Among thermoplastics, polystyrene was chosen in this study because it is easier to prepare homogeneous films with PS that can be used in charge generation measurements. Type-I CdSe/ZnSe QDs initially capped with oleic acid (OA) ligand was treated with pyridine to exchange the surface ligand.[88] Undoped polymers and QD-embedded polymers were contact charged by tapping with PTFE, and their charging propensities were displayed as the electrical voltage output measured upon tapping.

3.2.1. Characterizations of the Quantum Dots

QDs with oleic acid (OA) were prepared and characterized with UV-Vis, photoluminescence spectroscopy, fluorescence lifetime analysis, and TEM imaging. Size analysis of the QD core was made by using the reported equation in the literature [89] as 3.5 nm and further calculated by TEM analysis. TEM images of core CdSe and Type-I CdSe/ZnSe QDs capped with OA are given in Figure 3.4. As a result of TEM analysis, particle size and size distribution of the CdSe core were calculated as 3.4 ±

0.4 nm and 12.5 %, respectively. Size and size distribution of the type-I QDs were estimated as 5.4 nm ± 0.4 nm and 7.5%, respectively by using Image J program.

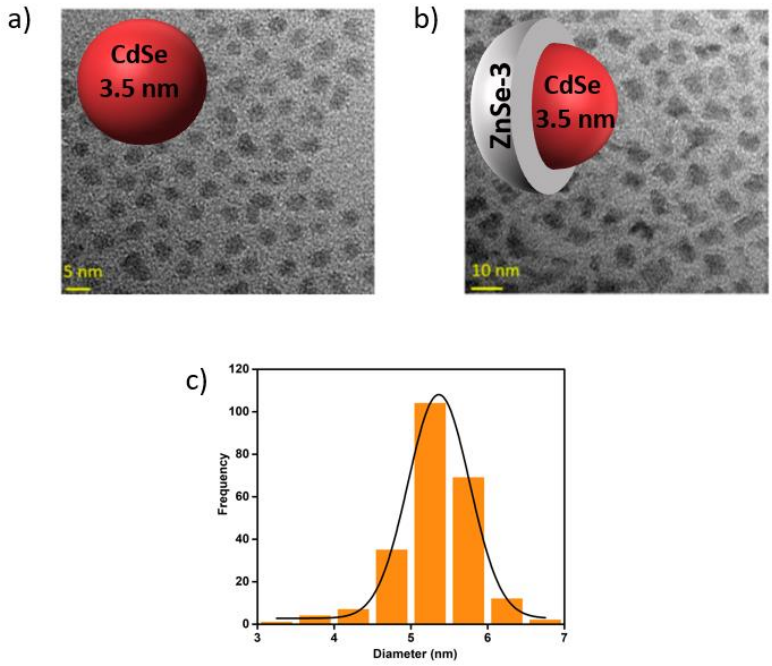

Figure 3.4. TEM images of QDs capped with oleic acid a) CdSe 3.5 nm, b) Type-I CdSe/ZnSe c) Size distribution curve of type-I CdSe/ZnSe. [83], [84]

Table 3.3. The maximum absorption and emission wavelengths of of CdSe/ZnSe QD (type-I) QDs with oleic acid ligand. [84]

QD	**Absorption ƛ max**	**Emission ƛ max**	**PL Quantum Yield**
CdSe/ZnSe QDs (type-I)	574 nm	587 nm	58.5 %

Lifetime of the QDs were measured by time-correlated single photon counting. The lifetime components were calculated by fitting the PL decay curve with a triple-exponential function given in the literature. [90] PL decay curves have a multiexponential nature, rendering their analysis complex due to competing radiationless processes including carrier trapping, charge transfer, etc. [91]

Table 3.4. Lifetime components taken from luminescence decay plot of CdSe/ZnSe QD (Type-I) QDs with oleic acid ligand. [84]

QD	τ_1 **(ns)**	τ_2 **(ns)**	τ_3 **(ns)**	τ_{av} **(ns)**
CdSe/ZnSe QD (Type-I)	1.46	6.53	20.27	12.61

τ_1, τ_2, and τ_3 represent the lifetimes. Among these lifetimes, short component corresponds to band edge excitons or single exciton, and fast component corresponds to charged exciton. [92], [93] The component τ_3 can be assigned to the deep trap site. Average lifetime τ_{av} is calculated based on the equations given in the literature. [91]

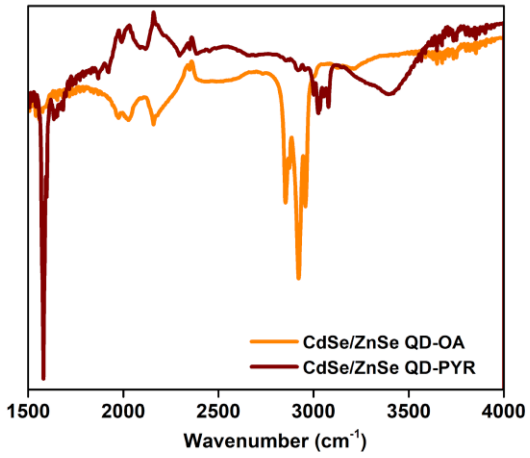

Figure 3.5. FTIR spectra of type-I CdSe/ZnSe QDs before (orange) and after (red) pyridine treatment. *

*Measured by Ms. Firdevs Aydın

FTIR spectra confirmed the ligand exchange procedure. FTIR spectra of type-I CdSe/ZnSe QD solution before and after pyridine treatment are shown in Figure 3.5.

The sharp peak observed at 1500 cm^{-1} and the peak at 3000-3500 cm^{-1} confirm the presence of pyridine molecules on the QDs surface.

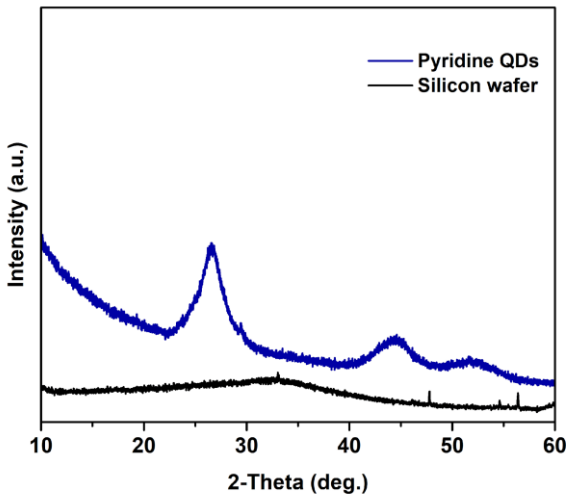

Figure 3.6. The X-ray diffractogram of pyridine treated QDs.

The solution of the QDs covered with pyridine was dropped cast on a silicon wafer (black) for XRD analysis and irritated copper Kα with 1.5418 Å wavelength. XRD of QDs are given in Figure 3.6. The diffraction angles were observed at 26.6, 44.6 and 52.4 degrees. The XRD pattern of CdSe shows peaks at 25.3, 42.1, and 49.7 degrees, which correspond to the lattice planes of (111), (220), and (311). [94] These peaks are shifted to the higher angles as shown in due to lattice compression of the core with the addition of ZnSe shell on the CdSe core material. [95]

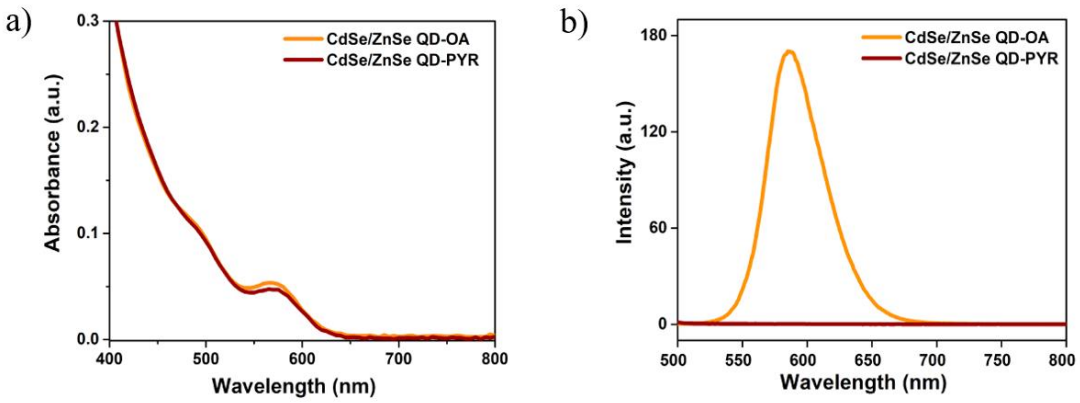

Figure 3.7. a) The UV-Vis absorbance and b) the photoluminescence spectra of type-I CdSe/ZnSe QDs before (orange) and after (red) pyridine treatment. *

*Measured by Ms. Firdevs Aydın

The absorbance and the photoluminescence spectra of the synthesized type-I CdSe/ZnSe QDs in hexane covered with oleic acid (OA) and pyridine (PYR) are shown in Figure 3.7. Absorption peak position remained unchanged with the pyridine treatment, indicating that there is no aggregation or oxidation as a result of the treatment. However, a significant decrease in the photoluminescence (PL) intensity was observed after the treatment. This decrease can be attributed to weaker surface passivation by pyridine molecules than OA. [88] Decrease in surface passivation may lead to an increase in non-radiative recombination processes.

3.2.2. Preparation and Characterization of the QD-doped Polystyrene

The composites were prepared as detailed in Section 2.5. In short, QD solution was stirred with the PS polymer solutions and the mixture was covered onto glass by dip coating.

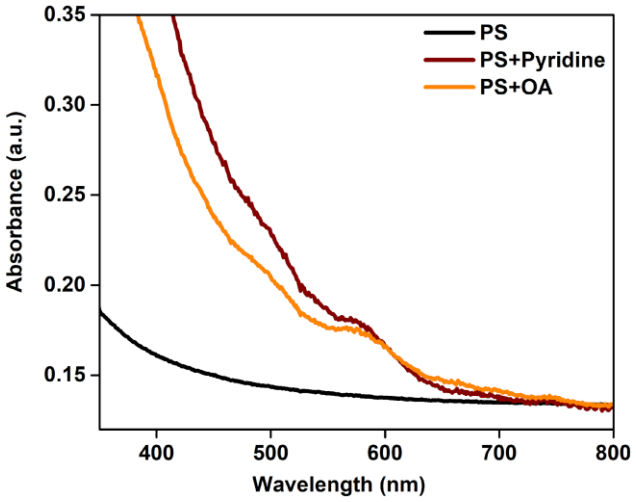

Figure 3.8. The absorbance spectra of the undoped and type-I CdSe/ZnSe QD doped PS; oleic acid (orange) and pyridine ligands (red) on the QDs.

The absorption maximum of the type-I CdSe/ZnSe QD (OA or PYR covered)-doped PS polymer was found as 574 nm as shown in Figure 3.8. The absorption peak position remained unchanged after the QD solution was doped into the polymer which can show that optical properties of the QDs were preserved.

3.2.3. Tapping Experiments with QD-PS and the Effect of Ligand-Exchange

Undoped PS polymer and QD-embedded PS polymers were contact charged with PTFE using the tapping device as described in Section 2.7.1 Contact and separation of the surfaces created open-circuit electrical potential signals. These signals are recorded as V_{oc} in mV using an oscilloscope attached to the tapping system. Measured potential signals are given in Figure 3.9.

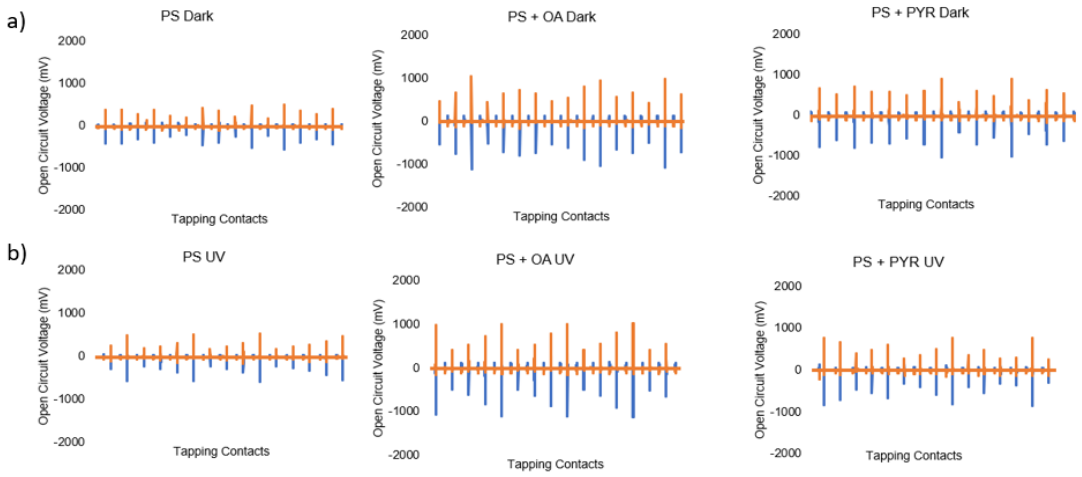

Figure 3.9. Contact and separation open-circuit potential (V_{oc}) signals from PS samples (blue) and PTFE (orange) a) in dark and b) under UV illumination.

Average values of the signals during contact were calculated for undoped and QD doped PS polymers are shown in Figure 3.10.

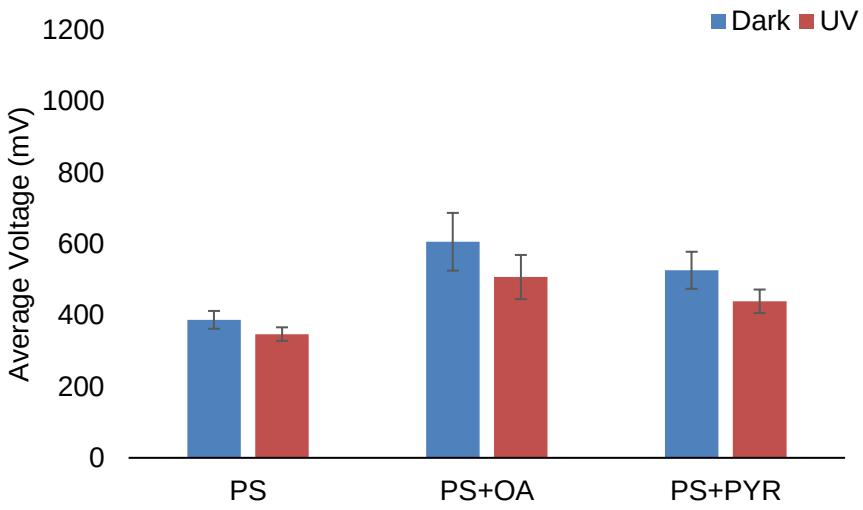

Figure 3.10. Average values of the open circuit potential maxima obtained during the tapping of PS and QD-PS with PTFE (shown in Figure 3.9). Error bars were calculated from at least three measurements for each case.

In dark, the average V_{oc} of the control PS sample was measured as 387 ± 25 mV, whereas PS doped with QD (capped with oleic acid (OA) and with pyridine (PYR)) led to an average V_{oc} values of 606 ± 81 mV, 526 ± 52 mV, respectively.

To investigate the effect of photoexcitation of the QDs on contact charge generation, tapping experiments were also conducted under UV illumination. UV light with a wavelength (390 nm), matching the absorbance characteristics of the QDs, was used for this setup. Under illumination, the average V_{oc} value of the control PS sample is 347 ± 19 mV, PS doped with QD (capped with oleic acid (OA) and with pyridine (PYR)) led to an average V_{oc} values of 507 ± 62 mV, 439 ± 33 mV, respectively.

3.2.4. Discussions

3.2.4.1. The effect of QD doping

The tapping experiments showed that adding type-I CdSe/ZnSe QDs (QDs) can improve the electrical voltage output up to 1.5 times (regardless of the type of ligand used) both under dark environment and UV illuminated conditions. As discussed in the introduction, contact-charged surfaces can undergo bond cleavage, which initiates the generation of mechanoions and mechanoradicals on the surface of polymers. One possible mechanism that can explain results is as follows: the electrons from PS mechanoions hop into the surface traps of the ZnSe shell and subsequently de-trap due to the close proximity of the PS's lowest unoccupied molecular orbital (LUMO) to the conduction band of ZnSe which leads to the stabilization of the charge, that is observed with the high Voc of the tapping with composites. It is also possible that QD additives may increase the number of mechanospecies formed by contact charging on the polymer surface. Increasing mechanospecies can cause an increase in overall open circuit voltage compared to undoped polymers.

3.2.4.2. The effect of Ligand Exchange

The molecular structure of pyridine comprises a six-membered ring with five carbon atoms and a nitrogen atom. The nitrogen atom in the ring retains a lone pair of electrons, whereas the oleic acid molecule has a long hydrocarbon chain with one double bond. Pyridine forms weak and reversible bonds with the surface cadmium ions of cadmium chalcogenide nanocrystals [96]. Therefore, it is a weaker stabilizing agent than OA and creates a thinner ligand shell. Consequently, one can expect an increase in the charge transfer between the QD and polymer with the QD capped with pyridine; however, the tapping experiments showed that the average voltage values of PS with QD capped with oleic acid (OA) and PS with QD capped with Pyridine (PYR) in dark were 507 ± 62 mV and 439 ± 33 mV, respectively. These values are quite close to each other, implying that ligand exchange did not create a significant effect in tribocharge generation.

Despite providing a thinner shell, the pyridine treatment could potentially have negligible effect on the charge transfer since the organization effects of the polymer chains around the QD are more dominant on charge generation than the chains of ligand.

Photoexcitation of quantum dots (QDs) can initiate the formation of excitons and increase the population of charge carriers [97] which could affect the measured voltage in the tapping experiments. Thus, we illuminated the QD-doped samples with UV light that matches their absorbance wavelength range (390 nm). UV illumination during the tapping experiments didn't affect contact charge generation compared to dark environment in our experiments. We hypothesize that charge generation is more related to mechanospecies formed on the polymer surface compared to effect of quantum dots.

3.3. QD Doping to Different Thermoplastic Polymers in Charge Generation

Quantum yield and size distribution of the synthesized QDs were calculated by Ms. Firdevs Aydın.

In our previous study, we demonstrated that quasi-type-II quantum dots (QDs) have more efficient interaction with mechanospecies generated on polymers compared to type-I heterostructured QDs. This better interaction is associated with the close proximity of charge carriers in quasi-type-II QDs to the polymer surface. [84] Therefore, the same quasi-type-II QDs were chosen for this study. QDs were doped in three common thermoplastic polymers: PS, PE, and PMMA to understand the changes in contact charging for the different polymers. Undoped and QD-doped polymers were tapped with PTFE, and their V_{oc} output were measured. Relative humidity during the measurements were recorded as 43%−45%.

3.3.1. Characterizations of the Quantum Dots

The absorbance and the photoluminescence spectra of the synthesized quasi-type-II CdSe/ZnSe QDs in hexane are shown in Figure 3.11.

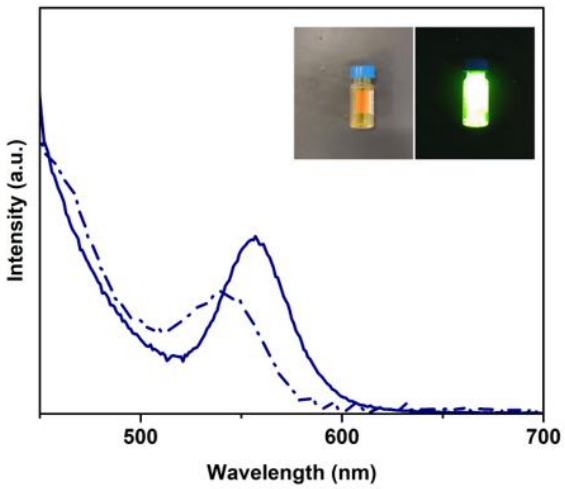

Figure 3.11. The absorbance (dashed line) and the photoluminescence spectra (solid line) of quasi-type-II CdSe/ZnSe QDs in hexane (excited at 450 nm)

The absorption and emission maxima of the quasi-type-II CdSe/ZnSe QD solution were found as 540 nm and 557 nm, respectively. (Table 3.5)

Table 3.5. The maximum absorption and emission wavelengths of the prepared QD solutions

QD	**Absorption ʎ max**	**Emission ʎ max**	**PL Quantum Yield**
CdSe/ZnSe (quasi-type-II)	540 nm	557 nm	43.9 %*

*Calculated by Ms. Firdevs Aydın

TEM images of core CdSe used in the synthesis of quasi-type-II CdSe/ZnSe QDs, and quasi-type-II CdSe/ZnSe QDs are given in Figure 3.12. The analyses of the TEM images using Image J program provided the values of the size and size distributions of

the CdSe core as 2.5 ± 0.2 nm and 9.2%, where for quasi-type-II QDs ; these values were found as 5.1 nm ± 0.4 nm and 7.8%.

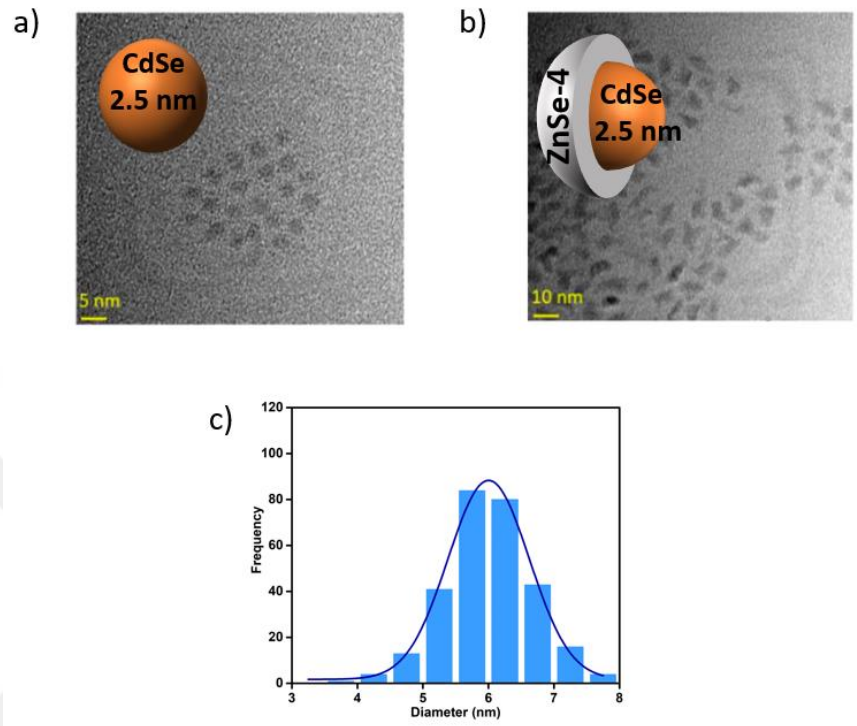

Figure 3.12. TEM images of a) CdSe 2.5 nm, b) CdSe/ZnSe (quasi-type-II) and c) The size distribution curve of quasi- type-II CdSe/ZnSe. [83], [84]

Lifetime of the QDs were measured by time-correlated single photon counting. The lifetime components were calculated by fitting the decay with a triple-exponential function. [90]

Table 3.6. Lifetime components obtained from decay plot of QDs

QD	τ_1 (ns)	τ_2 (ns)	τ_3 (ns)	τ_{av} (ns)
CdSe/ZnSe QD (quasi-type-II)	1.45	7.02	17.27	9.06

τ_1, τ_2, and τ_3 represent the lifetimes. Among these lifetimes, short component corresponds to band edge excitons or single exciton, and fast component corresponds to charged exciton. [92], [93] The component τ_3 can be assigned to the deep trap site. Average lifetime τ_{av} is calculated based on the equations given in the literature [91]

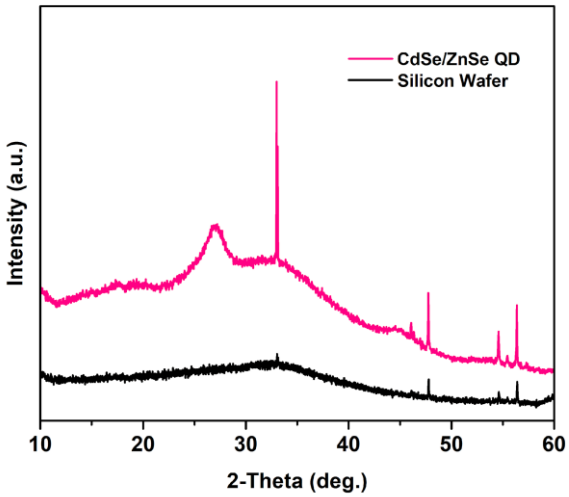

Figure 3.13. The X-ray diffractogram of quasi-type-II CdSe/ZnSe QDs.

The solution of quasi-type-II CdSe/ZnSe QDs was dropped cast on a silicon wafer (black) for XRD analysis and irritated with copper Kα having 1.5418 Å wavelength. The diffraction angles were observed at 27.20, 44.73, and 52.14. The XRD pattern of CdSe shows peaks at 25.3, 42.1, and 49.7 degrees, which correspond to the lattice planes of (111), (220), and (311) [94] these peaks are shifted to the higher angles due to lattice compression of the core with the addition of ZnSe shell on the CdSe core material. [95]

3.3.2. Preparation and Characterization of the QD-Doped Polymers

The composites were prepared as detailed in Section 2.6. In short, QD solutions were mixed with the polymer solutions. This mixture is further covered on the glass

substrates by the spin coating method to obtain a flat-surface sample. UV−visible (UV−Vis) and photoluminescence (PL) measurements of the 8.0 mg/mL QD doped PS, PE, or PMMA polymers and control samples (samples without QDs) were carried out to confirm the QD doping in the thermoplastics.

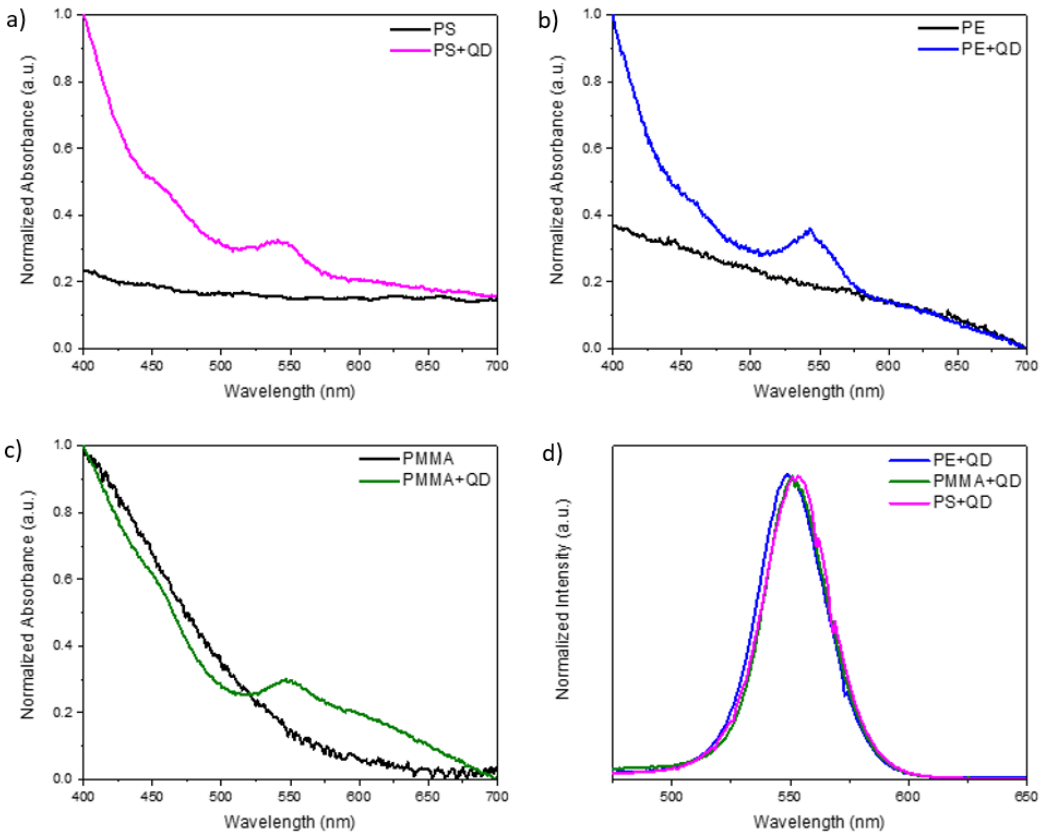

Figure 3.14. Optical properties of quasi-type-II CdSe/ZnSe thermoplastic nanocomposites. (a-c) The UV-Vis spectra of PS, PE, and PMMA nanocomposites respectively. d) Photoluminescence spectra of QD-doped nanocomposites excited at 450 nm.

Figure 3.14. illustrates the UV-VIS spectra and the photoluminescence spectra (excited at 450 nm) of nanocomposites. 8.0 mg/mL quasi-type-II CdSe/ZnSe doped thermoplastics have absorption and emission maxima of 545 nm and 555 nm respectively.

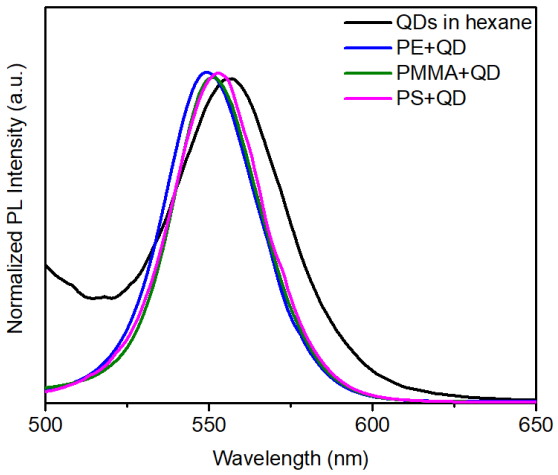

Figure 3.15. Photoluminescence spectra of QDs in solution and QD-doped nanocomposites excited at 450 nm.

Great amount of research has been done on preparing QD-polymer composites. [98]-[103] A previous study [100] demonstrated an approach to obtain photoluminescent CdSe/ZnS QD-PMMA composite films. They covered the QD–PMMA viscous composite solution by spin-coating on a glass lamel. They showed that the PMMA absorption occurs predominantly below 400 nm, and the absorption in the visible range was due to QDs, similar to QD-PMMA composites obtained in this thesis work.

Moreover, another study showed the preparation of fluorescent PE composites containing CdSe/ZnS quantum dots (QDs). [99] As a result of the study, the optical spectra of QDs in solution and QD-polymer composites were found to be similar, which shows that QDs preserved their properties after being embedded into the polymer. As seen from Figure 3.14 and Figure 3.15, prepared nanocomposites have similar absorbance and emission profiles to that of the QD solution, proving that QDs preserved their properties in the polymer composites, similar to the literature studies. [99] and [102]

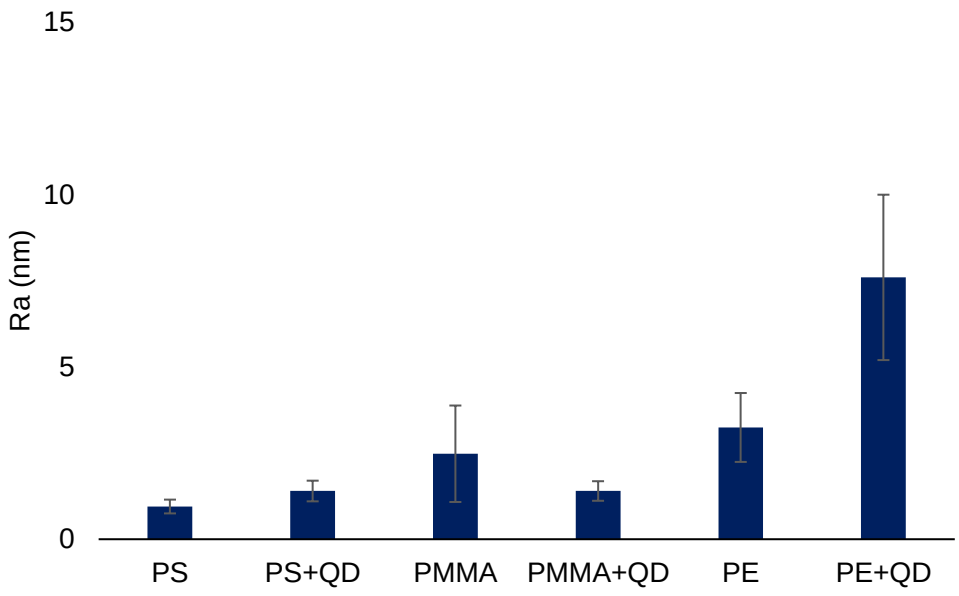

Figure 3.16. Average roughness (R_a) values of PS, PE and PMMA polymers with and without doped quasi-type-II CdSe/ZnSe quantum dots. The undoped samples were treated with the pure solvent instead of the QD solution.

Surface roughness values of the 8.0 mg/mL quasi-type-II CdSe/ZnSe doped polymers and the corresponding control samples (without QD) were obtained using AFM. The surface roughness did not change significantly with the addition of QDs, except for PE composites. The surface roughness of the QD-embedded PS, PE, and PMMA are found as 1.40 ± 0.30 nm, 7.6 ± 2.4 nm, and 1.40 ± 0.28 nm, whereas the surface roughness of PS, PE, and PMMA without QD are found as 0.95 ± 0.20 nm, 3.24 ± 1.00 nm and 2.48 ± 1.4 nm respectively Figure 3.16. Error bars represent the standard deviation of measurements of three samples for each case.

Table 3.7. Surface conductivities of QD-doped samples.

Material	**Conductivity (S)**
PMMA	1.03E-17
PMMA+QD	1.14E-17
PS	1.94E-17
PS+QD	2.63E-17
PE	4.1E-17
PE+QD	2.27E-17

The surface conductivities of control samples and 8.0 mg/mL QD-doped polymer samples were measured by the two-probe method (See section 2.7.2. for experimental details). The surface conductivity of the QD-doped polymers was found in the order of 10^{-17} S, which implies the samples are insulators, similar to the undoped control polymers. QD doping did not alter the insulator properties of polymers.

3.3.3. Tapping Experiments of the Thermoplastics

Contact charging experiments were conducted by tapping the undoped polymers and QD-doped polymers with PTFE. Contact electrification of the surfaces during contact and separation generated open-circuit electrical potential (V_{oc}) signals, recorded by the oscilloscope.

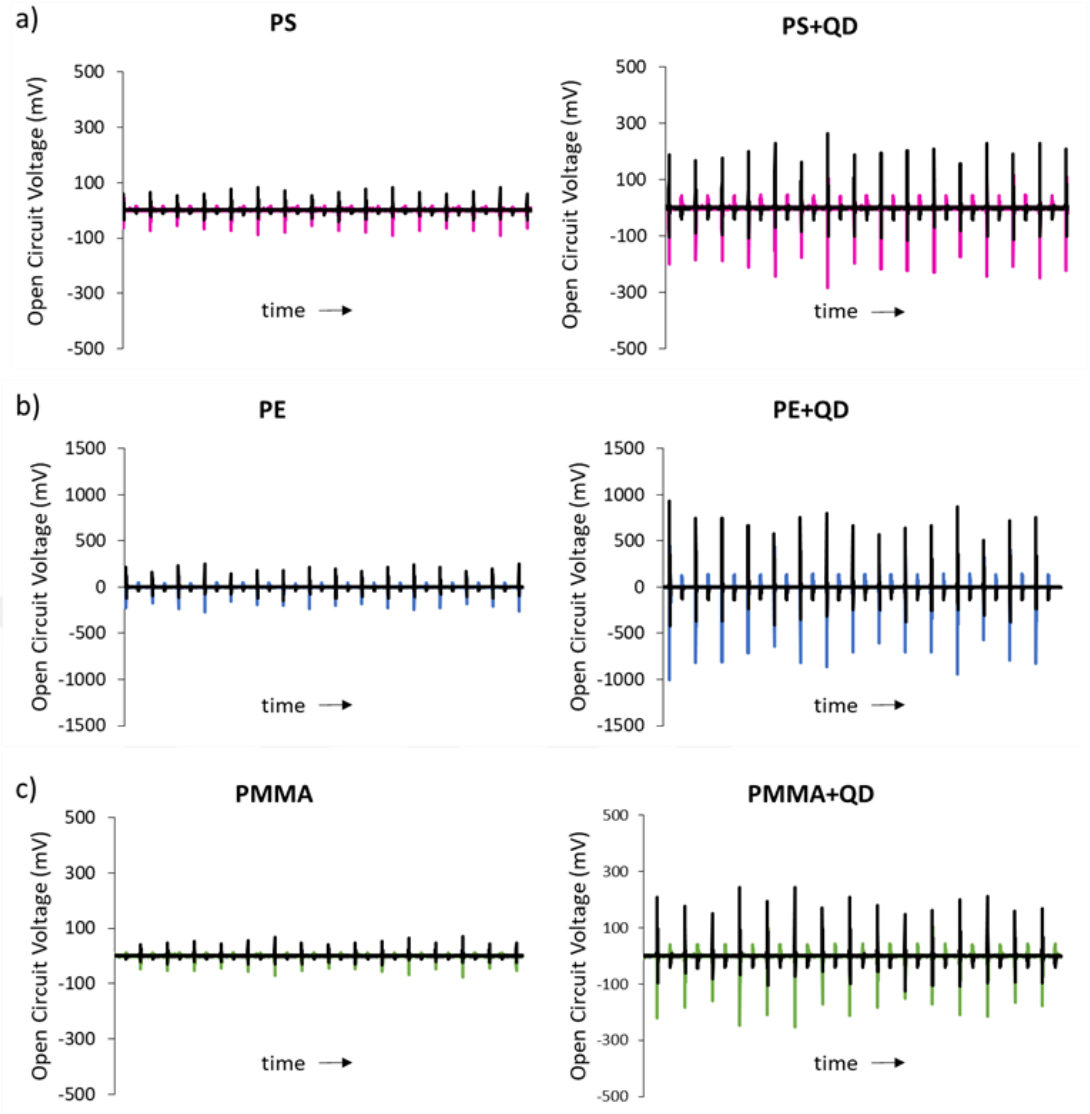

Figure 3.17 Open circuit voltage (V_{oc}) values obtained at the tapping device when polymers and their QD composites (8.0 mg/mL quasi-type-II CdSe/ZnSe) were tapped against polytetrafluoroethylene (PTFE) film. a) PS b) PE and c) PMMA.

PS control sample has average maximum V_{oc} value of 71 ± 1.6 mV and by the addition of 8.0 mg/mL QDs, this value increased to 213 ± 6.7 mV. For PE, the control sample has average maximum V_{oc} value of 215 ± 31 mV and by the addition of 8.0 mg/mL QDs, this value increased to 745 ± 11 mV. For PMMA and doped PMMA, these values were 54 ± 2.9 mV and 194 ± 3.7 mV, respectively.

Results demonstrated that quasi-type-II CdSe/ZnSe doping to polymers can significantly enhance the electrical voltage output by up to 5 times compared to the values observed in control experiments without quantum dots.

Quasi-type-II CdSe/ZnSe were also doped in different concentrations (2.0 mg/mL, 4.0 mg/mL, 6.0 mg/mL, 8.0 mg/mL solutions were used) to the polymers, and the composites were tapped in dark and under UV illumination (390 nm).

Average V_{oc} values obtained by tapping QD-embedded thermoplastics are shown in Figure 3.18, Figure 3.19 and Figure 3.20**.** Results are also summarized in Table 3.8. and Table 3.9.

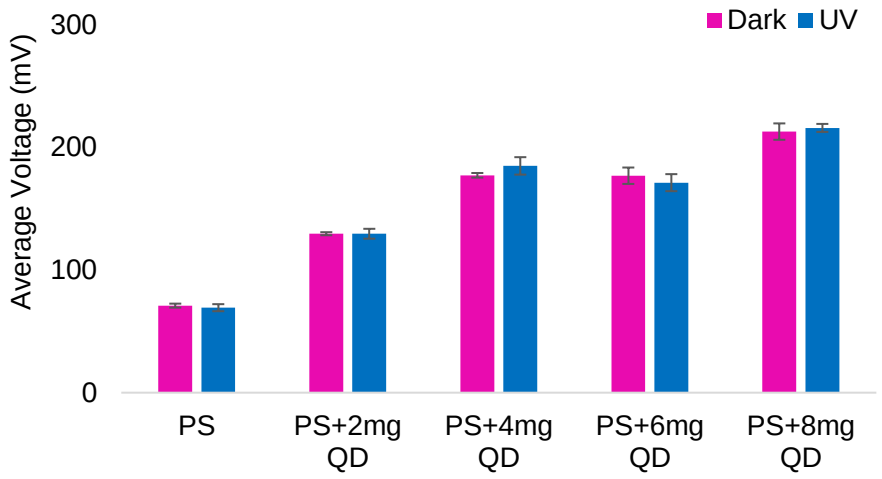

Figure 3.18. Average open-circuit potentials (V_{oc}) obtained by tapping PS polymer against PTFE in dark and under UV illumination, with different concentration of quasi-type-II CdSe/ZnSe doped into the polymer. Error bars correspond to standard deviations determined from at least three independent measurements.

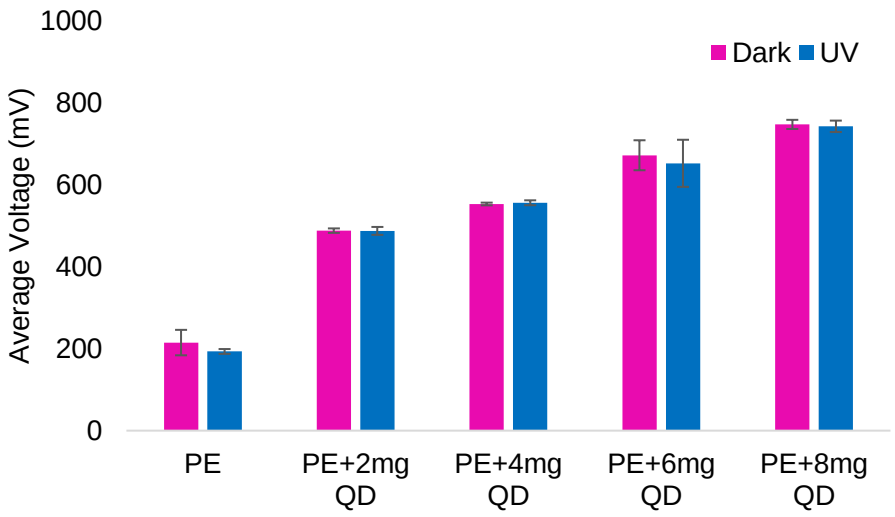

Figure 3.19. Average open-circuit potentials (V_{oc}) obtained by tapping PE polymer against PTFE in dark and under UV illumination, with different concentration of quasi-type-II CdSe/ZnSe doped into the polymer. Error bars correspond to standard deviations determined from at least three independent measurements.

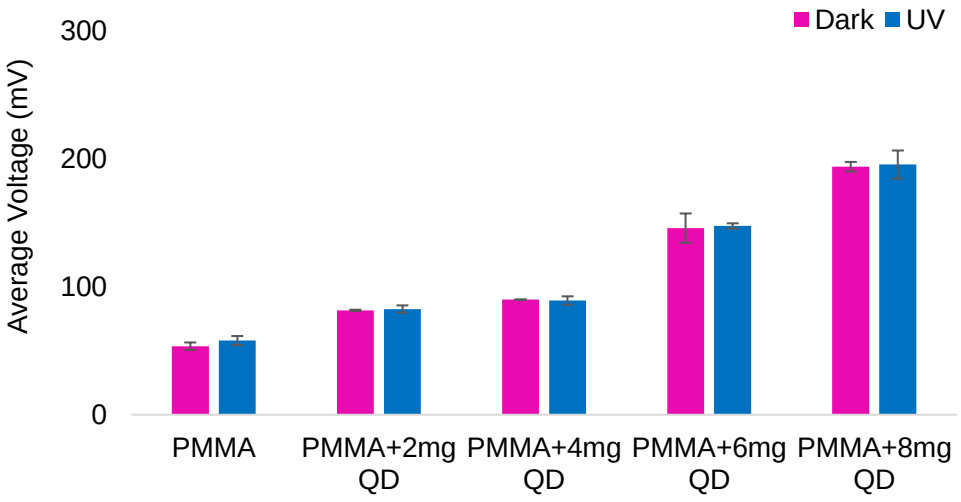

Figure 3.20. Average open-circuit potentials (V_{oc}) obtained by tapping PMMA polymer against PTFE in dark and under UV illumination, with different concentration of quasi-type-II CdSe/ZnSe doped into the polymer. Error bars correspond to standard deviations determined from at least three independent measurements.

Table 3.8. Average open-circuit potentials (V_{oc}) in mV obtained by tapping PS, PE and PMMA polymers against PTFE with different concentration of QDs embedded into the polymer in **dark**. Standard deviations are calculated from three independent measurements.

Polymer	Control	2.0 mg/mL QD	4.0 mg/mL QD	6.0 mg/mL QD	8.0 mg/mL QD
PS	71.0±1.63	130±1.25	177±1.89	177±6.68	213±6.68
PE	215±31.1	488±5.43	553±3.30	672±36.6	748±11.2
PMMA	53.7±2.87	81.7±0.47	90.0±0.00	146±11.4	194±3.74

Table 3.9. Average open-circuit potentials (V_{oc}) in mV obtained by tapping PS, PE and PMMA polymers against PTFE with different concentration of QDs embedded into the polymer **under UV illumination**. Standard deviations are calculated from three independent measurements.

Polymer	Control	2.0 mg/mL QD	4.0 mg/mL QD	6.0 mg/mL QD	8.0 mg/mL QD
PS	69.3±2.87	130±4.03	185±7.11	171±6.94	216±3.27
PE	193±5.91	488±9.67	556±6.02	653±57.5	743±19.9
PMMA	58±3.56	82.7±2.87	89.3±0	148±2.05	196±11.0

3.3.4. Discussions

The tapping experiments revealed that incorporating quasi-type-II CdSe/ZnSe QDs into thermoplastic polymers can significantly enhance the electrical voltage output in all three polymer matrices. And the electrical voltage output increases in parallel with the amount of QDs embedded in the polymers. UV illumination didn't show a significant difference in open circuit voltage compared to dark environment.

In accordance with the mechanism discussed in section 3.1.4. for type-I CdSe/ZnSe QD-PS nanocomposites, we propose that generated mechanoions on the polymer surfaces by tapping; can hop into the surface traps of the ZnSe shell and then de-trap due to the close proximity of the PS's lowest unoccupied molecular orbital (LUMO) to the conduction band of ZnSe which leads to an enhanced charge generation. Also, QD additives may enhance the formation of mechanospecies by contact charging on the polymer surface. Increasing the population of mechanospecies can increase overall open circuit voltage compared to undoped polymers.

3.4. N-CD Embedding to PVA Polymer

Carbon dots have recently gained interest for researchers due to their unique physicochemical properties, cost-effective, easy synthesis and biocompatibility compared to inorganic QDs. Nitrogen doping enhances the photoluminescent properties of carbon dots significantly by better passivating the surface. [104] Nitrogen-doped carbon dots and semiconductors have found various application fields; recently it was seen that the efficiency of solar cells can be increased by using nitrogen-doped semiconductors. [105] Nitrogen doping to graphene also showed increased power output in triboelectric nanogenerators (TENGs) [106].

Influenced by these enhanced properties from nitrogen doping, we investigated the role of N-doped Carbon Dots (N-CDs) by embedding them into poly (vinyl alcohol) (PVA) in contact charging. N-doped carbon dots were synthesized hydrothermally by reacting an aqueous Bovine Serum Albumin (BSA) solution as described in section 2.3. Because N-CDs are acquired in the form of aqueous solutions, we selected a water-soluble polymer, PVA, for this study to ensure compatibility with the solvent.

3.4.1. Synthesis and Characterizations of N-CDs

The absorbance and the photoluminescence spectra of the synthesized N-CDs in water are shown in Figure 3.21. The emission maxima of the solution was found as 430 nm. Absorbance and emission profiles of the N-CDs are found similar to the literature. [86]

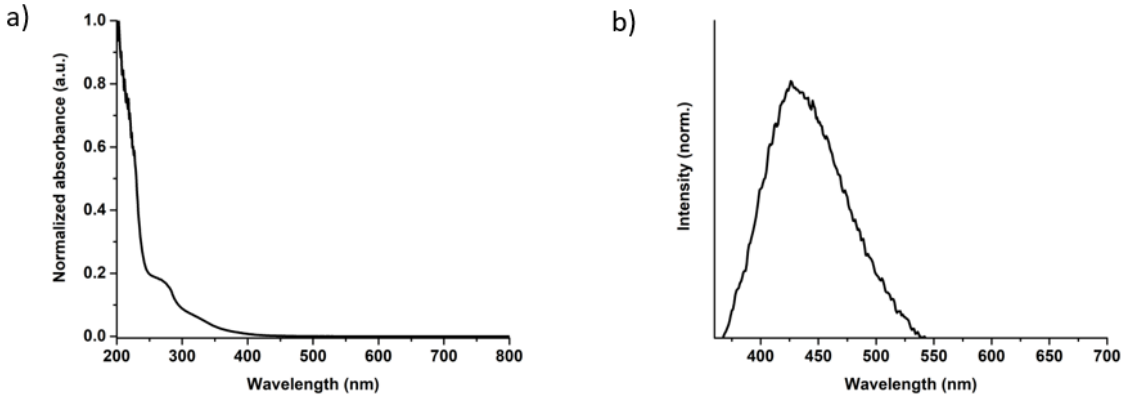

Figure 3.21. a) The absorbance and the b) photoluminescence spectra of the synthesized N-CD solutions in water (excited at 350 nm)

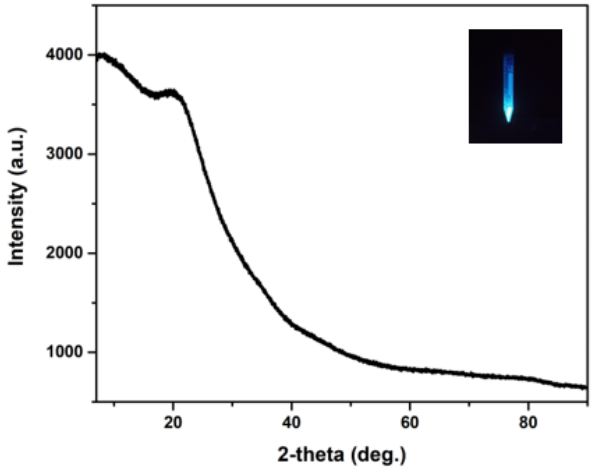

Figure 3.22. The X-ray diffractogram of lyophilized N-CD powder and the photo of powder N-CDs obtained from the synthesis (inset).

XRD spectra was recorded in the Materials Science (MS) beam-line at SESAME (Synchrotron-light for Experimental Science and Applications in the Middle East). N-CD aqueous solution obtained after the synthesis was lyophilized and inserted into a capillary tube. As seen in Figure 3.22. XRD pattern shows a peak at 22 degrees, which is due to the graphitic nature of carbon. [107]

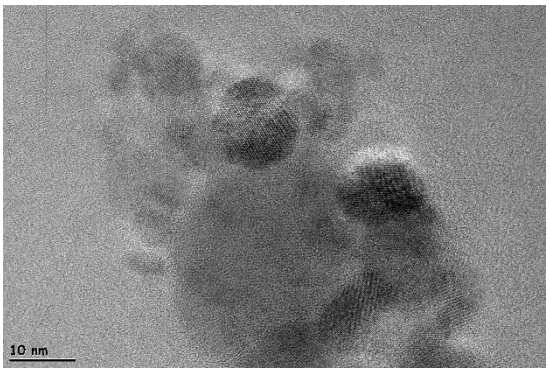

Figure 3.23. TEM images of N-CDs (Scale bar:10 nm)

N-CDs were found clustered together in the TEM images. Due to this clustering, an accurate size analysis of individual dots couldn’t be made.

3.4.2. Characterizations of N-CD Doped PVA

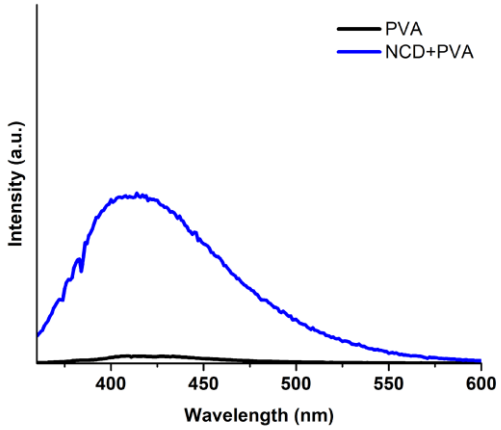

Figure 3.24. Photoluminescence spectra of N-CD embedded nanocomposites excited at 350 nm.

The photoluminescence spectra were found similar to the literature studies. [90] Energy-Dispersive X-ray Spectroscopy (EDX) analysis was performed for N-CD polymer films in SEM. The analysis confirms the presence of the nitrogen element in the PVA films.

a)

Atomic % by Element		
C	N	O
70.31	2.16	27.54

b)

Atomic % by Element		
C	N	O
56.24	22.25	21.51

Figure 3.25. EDX analysis results of a) PVA film b) PVA/N-CD composite film in volume ratio of 1:1

3.4.3. Charging Experiments of Polymers

Contact charging experiments were conducted by tapping the undoped polymers and N-CD-embedded polymers with aluminum stub. Contact electrification of the surfaces during contact and separation generated open-circuit electrical potential (V_{oc}) signals. These signals are recorded by using an oscilloscope. The V_{oc} values generated with tapping of the composites having PVA to N-CD ratio 1:0.25, 1:0.5 and 1:1 under ambient light is displayed in Figure 3.26.

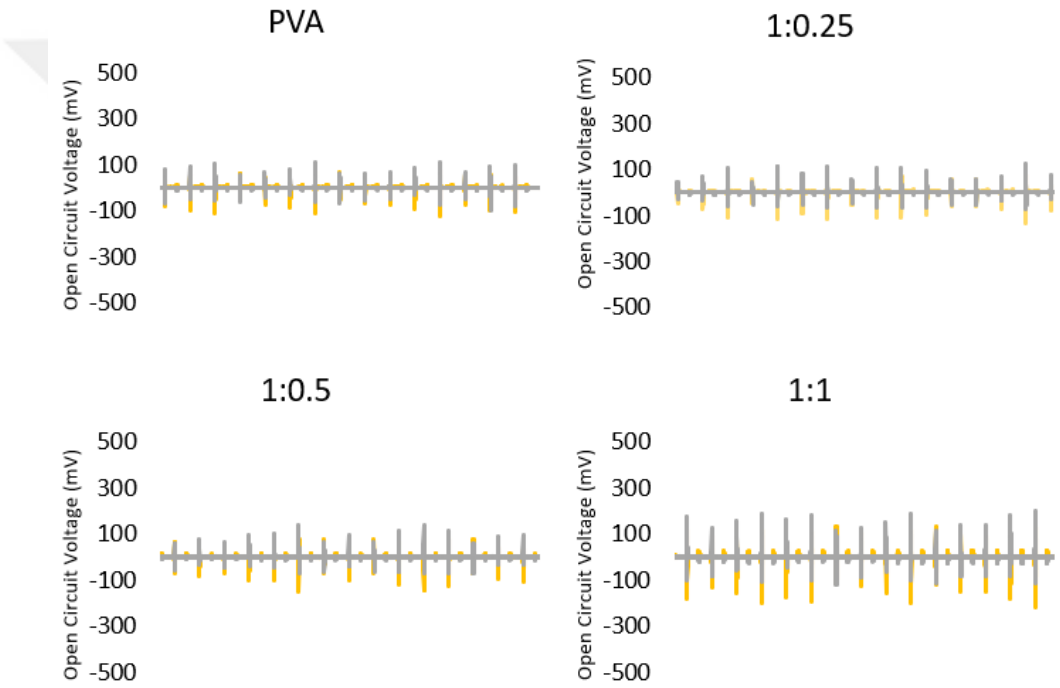

Figure 3.26. Open Circuit Voltage (V_{oc}) obtained upon tapping .a) PVA sample without N-CDs addition. b) PVA composite with PVA: N-CDs volume ratio 1:0.25 c) PVA composite with PVA: N-CDs volume ratio 1:0.5. d) PVA composite with PVA: N-CDs volume ratio 1:1. Tapping against aluminum stub at 1 Hz tapping frequency.

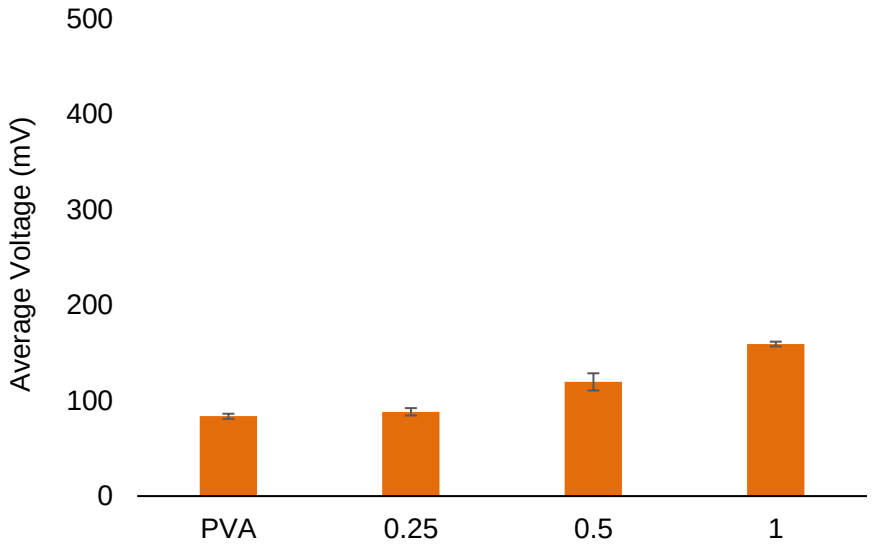

Figure 3.27. Average open-circuit potentials (V_{oc}) obtained by tapping PVA polymer against aluminum stub with different ratios of N-CDs embedded into the polymer. Error bars correspond to standard deviations determined from at least three independent measurements.

The average open-circuit potentials (V_{oc}) of the control PVA sample is measured as 84 ± 2.6 mV, PVA/N-CD film with PVA to N-CD volume ratio 1:0.25 is 88 ± 3.9 mV, 1:0.5 is 109 ± 9.0 mV, 1:1 is 159 ± 2.5 mV.

3.4.4. Discussions

In the initial experiments, it was observed that incorporating N-CD to PVA polymer led to an increase in the open circuit voltage achieved during tapping. However, a clustering issue was encountered in the synthesis of N-CD, as evident from the TEM image Figure 3.23. Further studies and characterization for the synthesis process are necessary. The clustering problem should be addressed to facilitate future research in this field.

Chapter 4

4. CONCLUSIONS AND FUTURE LOOK

In this thesis work, QDs were doped into some common polymers to investigate QD-polymer interactions regarding contact charging of the composites. Different heterostructures and surface properties of QDs were tested for their effect on contact electrification of the polymers. It was found that doping alloy QDs with different elemental ratios into PDMS affects the polymer charge stability: Alloy core/shell QDs can stabilize or destabilize the contact charges on the polymer surface depending on the different locations of the charge carriers (electrons and holes) on QDs. The charge mitigation rates can also be manipulated by UV illumination. Then, we demonstrated that changing the surface chemistry of QDs by ligand replacement, specifically oleic acid replaced by pyridine, had a negligible effect on the charge transfer, possibly due to the more dominant effect of polymer chains on charge transfer than ligand chains.

Then, we incorporated type-I and quasi-type-II CdSe/ZnSe QDs in thermoplastic polymers. The composites prepared were tapped to other surfaces in a homemade tapping device. In the three thermoplastic polymers we used as a matrix, the electrical voltage output obtained upon tapping increased with the doping of quasi-type-II QDs - both in the dark and under UV illumination. In the final part of the thesis, an attempt to use nitrogen-doped carbon dots as a dopant in PVA polymer was described. The clustering problem with nitrogen-doped carbon dots hampered us from seeing their effect on contact electrification. Further studies should be conducted to solve the clustering issue of carbon dots, and new elements could be used to investigate the effect of different heteroatom doping in contact electrification.

It was shown that the QD doping effect on contact charge decay rates with thermoplastics differed from that observed in PDMS. We attribute this difference to the thin samples we used to prepare the thermoplastic composites. Nevertheless, the main hypothesis that the QD-polymer interactions and the QD bandgap affect the charge stabilization on polymers is verified in each set we prepared. Therefore, this thesis work can be expanded in the future by using different sizes, types, and concentrations of quantum dots and other polymers to probe these interactions. In this study, we worked on two ligands only and detected no significant difference between the contact charging of the composites with QDs decorated with these ligands. The set of ligands can be enlarged to carefully design the QD-ligand-polymer interactions in future work. In addition, thermal degradation values of nanocomposites should be measured with thermal gravimetric analysis (TGA) to investigate the effect of QD doping into the polymers.

To sum up, the results have demonstrated that QDs can be used as potential antistatic dopants or charge enhancers in PDMS polymer and thermoplastic polymers. This work presents some preliminary efforts on understanding the mechanism of QD-polymer interactions in contact electrification of common polymers, which can lead to the development of future applications using nano-scale surface engineering of QDs.

REFERENCES

[1] A. Šutka et al., "Contact electrification between identical polymers as the basis for triboelectric/flexoelectric materials," *Phys. Chem. Chem. Phys.*, vol. 22, no. 23, pp. 13299–13305, 2020.

[2] M. M. Apodaca, P. J. Wesson, K. J. M. Bishop, M. A. Ratner, and B. A. Grzybowski, "Contact electrification between identical materials," *Angew. Chemie - Int. Ed.*, vol. 49, no. 5, 2010.

[3] R. G. Horn and D. T. Smith, "Dissimilar Materials," *Encycl. Therm. Stress.*, vol. 256, pp. 970–970, 2014.

[4] H. T. Baytekin, A. Z. Patashinski, M. Branicki, B. Baytekin, S. Soh, and B. A. Grzybowski, "The mosaic of surface charge in contact electrification," *Science*, vol. 333, no. 6040, pp. 308–312, 2011.

[5] U. G. Musa, S. D. Cezan, B. Baytekin, and H. T. Baytekin, "The Charging Events in Contact-Separation Electrification," *Sci. Rep.*, vol. 8, no. 1, 2018.

[6] X. Zhang, X. Huang, S. W. Kwok, and S. Soh, "Designing Non-charging Surfaces from Non-conductive Polymers," *Adv. Mater.*, vol. 28, no. 15, pp. 3024–3029, 2016.

[7] H. Baytekin, B. Baytekin, T. Hermans, B. Kowalczyk, and B. Grzybowski, "Control of Surface Charges by Radicals," *Science*, vol. 341, no. 6152, pp. 1368–1371, 2013.

[8] B. A. Kwetkus, "Particle triboelectrification and its use in the electrostatic separation process," *Part. Sci. Technol.*, vol. 16, no. 1, pp. 55–68, 1998.

[9] D. M. Pai and B. E. Springett, “Physics of electrophotography,” *Rev. Mod. Phys.*, vol. 65, no. 1, pp. 163–211, 1993.

[10] F. R. Fan, Z. Q. Tian, and Z. Lin Wang, “Flexible triboelectric generator,” *Nano Energy*, vol. 1, no. 2, pp. 328–334, 2012.

[11] B. Baytekin, H. T. Baytekin, and B. A. Grzybowski, “What really drives chemical reactions on contact charged surfaces?” *J. Am. Chem. Soc.*, vol. 134, no. 17, pp. 7223–7226, 2012.

[12] M. Sakaguchi, M. Makino, T. Ohura, and T. Iwata, “Contact electrification of polymers due to electron transfer among mechanoanions, mechanocations and mechano radicals,” *J. Electrostat.*, vol. 72, no. 5, pp. 412–416, 2014.

[13] M. Sakaguchi, Y. Miwa, and S. Hara, “Triboelectricity in polymers: effects of the ionic nature of carbon – carbon bonds in the polymer main chain on charge due to yield of mechano- anions produced by heterogeneous scission of the carbon – carbon bond by mechanical fracture,” *Journal of Development Economics.* vol. 62, pp. 35–50, 2004.

[14] H. T. Baytekin, B. Baytekin, J. T. Incorvati, and B. A. Grzybowski, “Material transfer and polarity reversal in contact charging,” *Angew. Chemie - Int. Ed.*, vol. 51, no. 20, 2012.

[15] J. Lowell, “The role of material transfer in contact electrification,” *J. Phys. D: Appl. Phys.* 10, L233, 1977.

[16] S. Matsusaka, H. Maruyama, T. Matsuyama, and M. Ghadiri, “Triboelectric charging of powders: A review,” *Chem. Eng. Sci.*, vol. 65, no. 22, pp. 5781–5807, 2010.

[17] W. Li, L. Ma, X. Xu, and J. Luo, “Bidirectional electron transfer in Triboelectrification caused by friction-induced change in surface electronic structure,” *Nano Energy*, vol. 114, no. April, p. 108667, 2023.

[18] L. S. McCarty and G. M. Whitesides, “Electrostatic charging due to separation of ions at interfaces: Contact electrification of ionic electrets,” *Angew. Chemie*, vol. 47, no. 12, pp. 2188–2207, 2008.

[19] D. J. Lacks and T. Shinbrot, “Long-standing and unresolved issues in triboelectric charging,” *Nature Reviews Chemistry*, vol. 3, no. 8. 2019.

[20] H. T. Baytekin, B. Baytekin, S. Soh, and B. A. Grzybowski, “Is water necessary for contact electrification?,” *Angew. Chemie* - Int. Ed., vol. 50, no. 30, 2011.

[21] K. P. Homewood, “Do ‘dirty’ surfaces matter in contact electrification experiments?” *J. Electrostat.*, vol. 10, no. C, pp. 299–304, 1981.

[22] M. Sakaguchi, M. Makino, T. Ohura, and T. Iwata, “Contact electrification of polymers due to electron transfer among mechanoanions, mechanocations and mechanoradicals,” *J. Electrostat.*, vol. 72, no. 5, pp. 412–416, 2014.

[23] R. K. Pandey, H. Kakehashi, H. Nakanishi, and S. Soh, “Correlating Material Transfer and Charge Transfer in Contact Electrification,” *J. Phys. Chem. C*, vol. 122, no. 28, pp. 16154–16160, 2018.

[24] Y. Fang, S. Gonuguntla, and S. Soh, “Universal Nature-Inspired Coatings for Preparing Noncharging Surfaces,” *ACS Appl. Mater. Interfaces*, vol. 9, no. 37, 2017.

[25] M. Özel, F. Demir, A. Aikebaier, J. Kwiczak-Yiğitbaşl, H. T. Baytekin, and B. Baytekin, “Why Does Wood Not Get Contact Charged? Lignin as an Antistatic Additive for Common Polymers,” *Chem. Mater.*, vol. 32, no. 17, pp. 7438–7444, 2020.

[26] S. D. Cezan, A. A. Nalbant, M. Buyuktemiz, Y. Dede, H. T. Baytekin, and B. Baytekin, “Control of triboelectric charges on common polymers by photoexcitation of organic dyes,” *Nat. Commun.*, vol. 10, no. 1, 2019.

[27] T. Mazur, B.A. Grzybowski, “Theoretical Basis for the Stabilization of Charges by Radicals on Electrified Polymers.” *Chem. Sci.*, vol. 8, pp. 7438–7444, 2017.

[28] P. C. Sherrell et al., “Probing Contact Electrification: A Cohesively Sticky Problem,” *ACS Appl. Mater. Interfaces*, vol. 13, no. 37, pp. 44935–44947, 2021.

[29] J. C. Wilcke, "Disputatio Physica Experimentalis, De Electricitatibus. Contrariis, Rostochii: Typis Ioannis Iacobi Adleri", 1757.

[30] J. Henniker, “Triboelectric in polymers” *Nature*, November 3, 1962, vol. 0, p. 1962, 1962.

[31] A. Coehn, “Ueber ein Gesetz der Electricitätserregung,” *Ann. Phys.*, vol. 300, no. 2, pp. 217–232, 1898.

[32] A. F. Diaz and R. M. Felix-Navarro, “A semi-quantitative tribo-electric series for polymeric materials: The influence of chemical structure and properties,” *J. Electrostat.*, vol. 62, no. 4, 2004.

[33] T. A. L. Burgo, T. R. D. Ducati, K. R. Francisco, K. J. Clinckspoor, F. Galembeck, and S. E. Galembeck, “Triboelectricity: Macroscopic charge patterns formed by self-arraying ions on polymer surfaces,” *Langmuir*, vol. 28, no. 19, 2012.

[34] T. Shinbrot, T. S. Komatsu, and Q. Zhao, “Spontaneous tribocharging of similar materials,” *Epl*, vol. 83, no. 2, 2008.

[35] R. F. Gouveia and F. Galembeck, “Electrostatic charging of hydrophilic particles due to water adsorption,” *J. Am. Chem. Soc.*, vol. 131, no. 32, pp. 11381–11386, 2009.

[36] A. Schella, S. Herminghaus, and M. Schröter, “Influence of humidity on tribo-electric charging and segregation in shaken granular media,” *Soft Matter*, vol. 13, no. 2, pp. 394–401, 2017.

[37] C. X. Lu et al., “Temperature Effect on Performance of Triboelectric Nanogenerator,” *Adv. Eng. Mater.*, vol. 19, no. 12, pp. 1–8, 2017.

[38] B. Düsenberg, F. Tischer, E. Valayne, J. Schmidt, W. Peukert, and A. Bück, “Temperature influence on the triboelectric powder charging during dry coating of polypropylene with nanosilica particles*,” Powder Technol.*, vol. 399, 2022.

[39] B. R. Conway and M. U. Ghori, “Triboelectrification of Pharmaceutical powders: A critical review,” *Br. J. Pharm.*, vol. 3, no. 1, 2018.

[40] S. Naik, R. Mukherjee, and B. Chaudhuri, “Triboelectrification: A review of experimental and mechanistic modeling approaches with a special focus on pharmaceutical powders,” *Int. J. Pharm.*, vol. 510, no. 1, pp. 375–385, 2016.

[41] H. Memon, H. Wang, S. Yasin, and A. Halepoto, “Influence of Incorporating Silver Nanoparticles in Protease Treatment on Fiber Friction, Antistatic, and Antibacterial Properties of Wool Fibers,” *J. Chem.*, vol. 2018, 2018.

[42] Y. Tian et al., “Carbon nanotube/polyurethane films with high transparency, low sheet resistance and strong adhesion for antistatic application,” *RSC Adv.*, vol. 7, no. 83, pp. 53018–53024, 2017.

[43] S. Kosiński, I. Rykowska, M. Gonsior, and P. Krzyżanowski, “Ionic liquids as antistatic additives for polymer composites – A review,” *Polym. Test.*, vol. 112, no. June, 2022

[44] P. Saini, V. Choudhary, and S. K. Dhawan, “Improved microwave absorption and electrostatic charge dissipation efficiencies of conducting polymer grafted fabrics prepared via in situ polymerization,” *Polym. Adv. Technol.*, vol. 23, no. 3, pp. 343–349, 2012

[45] S. D. Ekim, G. E. Kaya, M. Daştemir, E. Yildirim, H. T. Baytekin, and B. Baytekin, “Organic Charge Transfer Cocrystals as Additives for Dissipation of Contact Charges on Polymers,” *ACS Appl. Mater. Interfaces*, vol. 14, no. 50, pp. 56018–56026, 2022.

[46] B. D. Chen et al., “Au nanocomposite enhanced electret film for triboelectric nanogenerator,” *Nano Res.*, vol. 11, no. 6, pp. 3096–3105, 2018.

[47] K. Zhao et al., “Boosting power conversion efficiencies of quantum-dot-sensitized solar cells beyond 8% by recombination control,” *J. Am. Chem. Soc.*, vol. 137, no. 16, pp. 5602–5609, 2015.

[48] G. Khandelwal, N. P. M. Joseph Raj, N. R. Alluri, and S. J. Kim, “Enhancing Hydrophobicity of Starch for Biodegradable Material-Based Triboelectric Nanogenerators,” *ACS Sustain. Chem. Eng.*, vol. 9, no. 27, pp. 9011–9017, 2021.

[49] S. Joo et al., “Eco-Friendly Keratin-Based Additives in the Polymer Matrix to Enhance the Output of Triboelectric Nanogenerators,” *ACS Appl. Bio Mater.*, vol. 5, no. 12, pp. 5706–5715, 2022.

[50] G. J. Choi, S. H. Baek, S. S. Lee, F. Khan, J. H. Kim, and I. K. Park, “Performance enhancement of triboelectric nanogenerators based on polyvinylidene fluoride/graphene quantum dot composite nanofibers,” *J. Alloys Compd.*, vol. 797, pp. 945–951, 2019.

[51] V. I. Srdanov, N. P. Blake, D. Markgraber, H. Metiu, and G. D. Stucky, “Alkali Metal and Semiconductor Clusters in Zeolites*”, C. Elsevier Masson SAS*, vol. 85, 1994.

[52] B. Gidwani et al., “Quantum dots: Prospectives, toxicity, advances and applications,” *J. Drug Deliv. Sci. Technol.*, vol. 61, no. May 2020, p. 102308, 2021.

[53] A. C. Berends and C. De Mello Donega, “Ultrathin One- and Two-Dimensional Colloidal Semiconductor Nanocrystals: Pushing Quantum Confinement to the Limit,” *J. Phys. Chem. Lett.*, vol. 8, no. 17, pp. 4077–4090, 2017.

[54] G. S. Selopal, H. Zhao, Z. M. Wang, and F. Rosei, “Core/Shell Quantum Dots Solar Cells,” *Adv. Funct. Mater.*, vol. 30, no. 13, 2020.

[55] R. Zhou et al., “Tailoring band structure of ternary CdSxSe1-x quantum dots for highly efficient sensitized solar cells,” *Sol. Energy Mater. Sol. Cells*, vol. 155, pp. 20–29, 2016.

[56] M. L. H. Green, “A new approach to the formal classification of covalent compounds of the elements,” *J. Organomet. Chem.*, vol. 500, no. 1–2, pp. 127–148, 1995.

[57] F. Schreiber, “Structure and growth of self-assembling monolayers,” *Prog. Surf. Sci.*, vol. 65, no. 5–8, pp. 151–257, 2000.

[58] P. Schapotschnikow, B. Hommersom, and T. J. H. Vlugt, “Adsorption and binding of ligands to cdse nanocrystals,” *J. Phys. Chem. C*, vol. 113, no. 29, pp. 12690–12698, 2009.

[59] R. Rossetti and L. Brus, “Electron-hole recombination emission as a probe of surface chemistry in aqueous CdS colloids,” *J. Phys. Chem.*, vol. 86, no. 23, pp. 4470–4472, 1982.

[60] A. P. Alivisatos, “Birth of a nanoscience building block,” *ACS Nano*, vol. 2, no. 8, pp. 1514–1516, 2008.

[61] H. P. Rocksby, *J. Soc. Glass Technol.* 16, 171, 1932.

[62] A. I. Ekimov, A. L. Efros, and A. A. Onushchenko, “Quantum size effect in semiconductor microcrystals,” *Solid State Commun.*, vol. 56, no. 11, pp. 921–924, 1985.

[63] H. Weller, “Colloidal Semiconductor Q-Particles: Chemistry in the Transition Region Between Solid State and Molecules,” *Angew. Chemie Int. Ed. English*, vol. 32, no. 1, pp. 41–53, 1993.

[64] C. B. Murray, D. J. Norris, and M. G. Bawendi, “Synthesis and Characterization of Nearly Monodisperse CdE (E = S, Se, Te) Semiconductor Nanocrystallites,” *J. Am. Chem. Soc.*, vol. 115, no. 19, pp. 8706–8715, 1993.

[65] C. Y. Han, H. S. Kim, and H. Yang, “Quantum dots and applications,” *Materials*, vol. 13, no. 4, 2020.

[66] I. J. Kramer and E. H. Sargent, “Colloidal quantum dot photovoltaics: A path forward,” *ACS Nano*, vol. 5, no. 11, pp. 8506–8514, 2011.

[67] A. Valizadeh et al., “Quantum dots: Synthesis, bioapplications, and toxicity,” *Nanoscale Res. Lett.*, vol. 7, pp. 19–21, 2012.

[68] H. Liu et al., “Near-infrared lead chalcogenide quantum dots: Synthesis and applications in light emitting diodes,” *Chinese Phys. B*, vol. 28, no. 12, 2019.

[69] Y. Sun et al., “Quantum-Sized Carbon Dots for Bright and Colorful Photoluminescence,” *Journal of the American Chemical Society*, pp. 7756–7757, 2006.

[70] M. Bottini, C. Balasubramanian, M. I. Dawson, A. Bergamaschi, S. Bellucci, and T. Mustelin, “Isolation and Characterization of Fluorescent Nanoparticles from Pristine and Oxidized Electric Arc-Produced Single-Walled Carbon Nanotubes,” *J. Phys Chem B.* pp. 831–836, 2006.

[71] Q. Zhao, Z. Zhang, B. Huang, J. Peng, and M. Zhang, “Facile preparation of low cytotoxicity fluorescent carbon nanocrystals by electrooxidation of graphite w,” *Chem. Commun.* pp. 5116–5118, 2008.

[72] F. Wang, S. Pang, L. Wang, and Q. Li, “One-Step Synthesis of Highly Luminescent Carbon Dots in Noncoordinating Solvents,” *Chem. Mater.* no. 21, pp. 4528–4530, 2010.

[73] A. N. Kapitonov, M. N. Egorova, A. E. Tomskaya, S. A. Smagulova, and A. A. Alekseev, “Hydrothermal synthesis of carbon dots and their luminescence,” *AIP Conf. Proc.*, vol. 2041, 2018.

[74] W. Su et al., “Carbon dots: A booming material for biomedical applications,” *Mater. Chem. Front.*, vol. 4, no. 3, pp. 821–836, 2020.

[75] Q. Xu et al., “Heteroatom-doped carbon dots: synthesis, characterization, properties, photoluminescence mechanism and biological applications,” *J. Mater. Chem. B*, vol. 4, no. 45, pp. 7204–7219, 2016.

[76] V. M. Naik, S. V. Bhosale, and G. B. Kolekar, “A brief review on the synthesis, characterisation and analytical applications of nitrogen doped carbon dots,” *Anal. Methods*, vol. 14, no. 9, pp. 877–891, 2022.[3]

[77] Q. Zaman, K. M. Zia, M. Zuber, Y. N. Mabkhot, F. Almalki, and T. Ben Hadda, “A comprehensive review on synthesis, characterization, and applications of polydimethylsiloxane and copolymers,” *Int. J. Plast. Technol.*, vol. 23, no. 2, pp. 261–282, 2019.

[78] H. T. Baytekin, B. Baytekin, and B. A. Grzybowski, “Mechanoradicals created in ‘polymeric sponges’ drive reactions in aqueous media,” *Angew. Chemie - Int. Ed.*, vol. 51, no. 15, pp. 3596–3600, Apr. 2012.

[79] L. Ģērmane, L. Lapčinskis, M. Iesalnieks, and A. Šutka, “Surface engineering of PDMS for improved triboelectrification,” *Mater. Adv.*, vol. 4, no. 3, pp. 875–880, 2023.

[80] M. P. Wolf, G. B. Salieb-Beugelaar, and P. Hunziker, “PDMS with designer functionalities—Properties, modifications strategies, and applications,” *Prog. Polym. Sci.*, vol. 83, pp. 97–134, 2018.

[81] M.J. Owen, “Elastomers : Siloxane,” pp. 6–8, 2001.

[82] Statista, " Production forecast of thermoplastics worldwide from 2020 to 2050, by type" Available: https://www.statista.com/statistics/1192886/thermoplastics-production-volume-by-type-globally/ [Accessed: 16-08-2023]

[83] S.D. Ekim, "Control of Contact Charging on Polymers with Organic Charge-Transfer Complexes and Quantum Dots" M.S. thesis, Bilkent University, Ankara, Turkey, 2022.

[84] Ekim, S.D.; Aydin, F.; Kaya, G.E.; Baytekin, H. T.; Alptekin D.A.; Baytekin, B. Rise and Fall of Contact Charges on Polymers with Embedded Quantum Dots. [Manuscript under review]

[85] V. B. Kumar, J. Sheinberger, Z. Porat, Y. Shav-Tal, and A. Gedanken, "A hydrothermal reaction of an aqueous solution of BSA yields highly fluorescent N doped C-dots used for imaging of live mammalian cells," *J. Mater. Chem. B*, vol. 4, no. 17, pp. 2913–2920, 2016.

[86] V. B. Kumar, A. K. Sahu, A. S. M. Mohsin, X. Li, and A. Gedanken, "Refractive-Index Tuning of Highly Fluorescent Carbon Dots," *ACS Appl. Mater. Interfaces*, vol. 9, no. 34, pp. 28930–28938, 2017.

[87] K. V. Vokhmintcev, P. S. Samokhvalov, and I. Nabiev, "Charge transfer and separation in photoexcited quantum dot-based systems," *Nano Today*, vol. 11, no. 2, pp. 189–211, 2016.

[88] I. Lokteva, N. Radychev, F. Witt, H. Borchert, J. Parisi, and J. Kolny-Olesiak, "Surface treatment of cdse nanoparticles for application in hybrid solar cells: The effect of multiple ligand exchange with pyridine," *J. Phys. Chem. C*, vol. 114, no. 29, pp. 12784–12791, 2010.

[89] W. W. Yu, L. Qu, W. Guo, and X. Peng, “Experimental Determination of the Extinction Coefficient of CdTe , CdSe , and CdS Nanocrystals,” *Chem. Mater.* vol. 125, no. 17, pp. 2854–2860, 2003.

[90] M. S. Mehata and R. K. Ratnesh, “Luminescence properties and exciton dynamics of core-multi-shell semiconductor quantum dots leading to QLEDs,” *Dalt. Trans.*, vol. 48, no. 22, pp. 7619–7631, 2019.

[91] H. Kudilatt, B. Hou, and M. E. Welland, “Quantum Dots Microstructural Metrology: From Time-Resolved Spectroscopy to Spatially Resolved Electron Microscopy,” *Part. Part. Syst. Charact.*, vol. 37, no. 12, pp. 1–21, 2020.

[92] A. Javier, D. Magana, T. Jennings, and G. F. Strouse, “Nanosecond exciton recombination dynamics in colloidal CdSe quantum dots under ambient conditions,” *Appl. Phys. Lett.*, vol. 83, no. 7, pp. 1423–1425, 2003.

[93] U. Kaiser, D. Jimenez De Aberasturi, R. Malinowski, F. Amin, W. J. Parak, and W. Heimbrodt, “Multiplexed measurements by time resolved spectroscopy using colloidal CdSe/ZnS quantum dots,” *Appl. Phys. Lett.*, vol. 104, no. 4, 2014.

[94] J. Hao et al., “A facile route to synthesize CdSe / ZnS thick-shell quantum dots with precisely controlled green emission properties: towards QDs based LED applications,” *Sci. Rep.*, no. February, pp. 1–8, 2019.

[95] J. Zhu et al., “Highly efficient wurtzite/zinc blende CdS visible light photocatalyst with high charge separation efficiency and stability,” *J. Chem. Phys.*, vol. 152, no. 24, 2020.

[96] X. Ji, D. Copenhaver, C. Sichmeller, and X. Peng, “Ligand bonding and dynamics on colloidal nanocrystals at room temperature: The case of alkylamines on CdSe nanocrystals,” *J. Am. Chem. Soc.*, vol. 130, no. 17, pp. 5726–5735, 2008.

[97] K. V. Vokhmintcev, P. S. Samokhvalov, and I. Nabiev, “Charge transfer and separation in photoexcited quantum dot-based systems” *Nano Today*, vol. 11, no. 2, pp. 189-211, 2016.

[98] F. Meinardi et al., “Large-area luminescent solar concentrators based on Stokes-shift-engineered nanocrystals in a mass-polymerized PMMA matrix,” *Nat. Photonics*, vol. 8, no. 5, pp. 392–399, 2014.

[99] A. Bobrovsky, V. Shibaev, G. Elyashevitch, K. Mochalov, and V. Oleynikov, “Polyethylene-based composites containing high concentration of quantum dots,” *Colloid Polym. Sci.*, vol. 293, no. 5, pp. 1545–1551, 2015.

[100] H. Song and S. Lee, “Photoluminescent (CdSe) ZnS quantum dot-polymethylmethacrylate polymer composite thin films in the visible spectral range,” *Nanotechnology*, vol. 18, no. 5, 2007.

[101] Weaver, R. Zakeri, S. Aouadi, and P. Kohli, “Synthesis and characterization of quantum dot-polymer composites,” *J. Mater. Chem.*, vol. 19, no. 20, pp. 3198–3206, 2009.

[102] W. G. Lawrence, S. Thacker, S. Palamakumbura, K. J. Riley, and V. V. Nagarkar, “Quantum dot-organic polymer composite materials for radiation detection and imaging,” *IEEE Trans. Nucl. Sci.*, vol. 59, no. 1, pp. 215–221, 2012.

[103] H. Gordillo, I. Surez, R. Abargues, P. Rodrguez-Cant, S. Albert, and J. P. Martnez-Pastor, "Polymer/QDs nanocomposites for waveguiding applications," *J. Nanomater.*, vol. 2012, 2012.

[104] J. Manioudakis et al., "Effects of nitrogen-doping on the photophysical properties of carbon dots," *J. Mater. Chem. C*, vol. 7, no. 4, pp. 853–862, 2019.

[105] D. Carolan, C. Rocks, D. B. Padmanaban, P. Maguire, V. Svrcek, and D. Mariotti, "Environmentally friendly nitrogen-doped carbon quantum dots for next generation solar cells," *Sustain. Energy Fuels*, vol. 1, no. 7, pp. 1611–1619, 2017.

[106] G. Pace et al., "Nitrogen-doped graphene based triboelectric nanogenerators," *Nano Energy*, vol. 87, no. March, 2021.

[107] C. Jiang, H. Wu, X. Song, X. Ma, J. Wang, and M. Tan, "Presence of photoluminescent carbon dots in Nescafe® original instant coffee: Applications to bioimaging," *Talanta*, vol. 127, pp. 68–74, 2014.